An Investigation of Shearing Flows of Newtonian and Non-Newtonian Fluids

Group 22 M2R Report

Ping Zhu, Derek Ma, Jackie Li, Felicia Li, Samuel Yiu

Department of Mathematics
Imperial College London
June 2023

Abstract

We examine the velocity profiles for Newtonian fluids in rectilinear shearing flows between parallel plates and through a cylindrical tube. The Oldroyd-B model is employed to explore changes in these profiles when the fluid exhibits viscoelastic properties, and cases of shear-thinning/thickening fluids are also touched upon. In particular, we develop a simplistic model for blood flow through an artery as a viscoelastic fluid under a periodic pressure gradient. We conclude with a study of the Weissenberg effect, highlighting a key difference between Newtonian and viscoelastic fluids.

Contents

Nomenclature

For clarity, we provide a list of some basic symbols and conventions employed throughout the report. More complex notation will be introduced where appropriate.

$\delta(x)$	Dirac delta function
δ_{ij}	Kronecker delta
γ_E	Euler-Mascheroni constant
$\mathcal{F}\{f\}$	Fourier transform in one of the variables of a (possibly multivariate) function f
ω_j	An angular frequency of oscillation - the j is arbitrary and included to distinguish from ω arising in Fourier transforms
$\overline{z}$	Complex conjugate of z
$\partial_x f$	Partial derivative of f with respect to x
ρ	(Constant) density of the fluid under study
g	Gravitational acceleration on Earth
H	Separation (or half the separation, depending on context) of parallel plates
H_m	m^{th} harmonic number
R	Radius of cylindrical tube
η	Viscosity of a fluid - the amount which the fluid resists the shearing motion.

1 Introduction

Fluids are omnipresent. Any substance that flows, i.e. continuously deforms when acted upon by a force, is a fluid, including all gases and liquids, and even substances which we consider as solids in normal circumstances, such as glass. It is therefore clear that the study of fluids is remarkably diverse in variety and applications.

Fluids come in many flavours, the simplest being the Newtonian fluid, of which water is the paradigmatic example. However, these fluids per se are relatively uninteresting, though their flows can demonstrate complex behaviour. In this report we compare Newtonian fluids to other flavours of fluids - broadly termed non-Newtonian fluids, which can exhibit intriguing properties. In particular, we consider two cases separately - where the fluid is viscoelastic, which in our context is when long chain polymers are dissolved in a Newtonian solvent; and inelastic with $\dot{\gamma}$-dependent viscosity. Of course, in real life many fluids are much more sophisticated, and often display many of these properties together.

There exist a number of elementary shearing flows which are frequently studied, two examples of which are the Couette flow and Poiseuille flow, which constitute the focus of section 2. A shear flow is simply one in which parallel layers of the fluid flow past each other at varying velocities. We also examine more elaborate situations, where the plates are in oscillation, and the case of a simplified blood flow model with a periodic pressure gradient, which will bear similarity to and draw on many techniques from previous sections. For each of these physical configurations, we will carry out quantitative analysis of the flows of fluids with different properties, primarily between Newtonian and viscoelastic fluids, but also with power-law and Carreau fluids (see section 1.1, Non-Newtonian fluids) by solving for their velocity profiles. These will depend on parameters such as the viscosity, density and possibly the presence of polymers and their properties, as well as other physical conditions. We highlight some of them below.

In each model, we will make the following assumptions:

1. The plates/tube in which the fluid flows in is boundless
2. There is 'no-slip' (the velocity of the fluid at the boundary is equal to the boundary condition)
3. The flow is laminar
4. The flow is fully developed (velocity field is constant in direction of motion)
5. The fluid is incompressible (its density is constant).

While these constraints limit our models significantly, they ensure that the problems we consider are solvable analytically. Where these constraints are relaxed, we approach the problems numerically.

Finally, using some of the theory developed for the blood flow problem, we turn to study the 'rod climbing', or Weissenberg, effect, which will illustrate a case where viscoelastic properties of the fluid can cause it to behave in a manner contrary to that of Newtonian fluids.

At this point it will be necessary to clarify a few terms and pieces of notation. In the conventional sense a vector can be seen as a 1st-order tensor, a matrix a 2nd-order tensor and so on. So from here, we will use 'tensor', 'vector' and 'matrix' interchangeably where it is clear from context what we are referring to.

We will often refer to a quantity known as the shear rate, which is the rate of change of velocity across the layers, defined [2]

$$\dot{\gamma} = \sqrt{2\mathbf{E} : \mathbf{E}} \tag{1.0.1}$$

where

$$\mathbf{E} = \frac{1}{2}(\nabla \mathbf{u} + (\nabla \mathbf{u})^T) \tag{1.0.2}$$

is known as the rate of strain tensor, and the colon symbol denotes a double dot product. The above is a general definition - we will find that throughout the report, it is often the case that this reduces to $\dot{\gamma} = \partial_y u_x$.

We also have the stress tensor $\boldsymbol{\sigma}$, which encapsulates the stress forces experienced by the fluid. Consider an infinitesimally small fluid element. The ij^{th} element of $\boldsymbol{\sigma}$ ($\boldsymbol{\sigma}_{ij}$) is the force acting on the surfaces of the cube normal to the i^{th} direction, acting in the j^{th} direction. This is illustrated in the diagram below (Figure 1, based on [3, Kundu]). We will tacitly identify 1, 2, 3 with x, y, z henceforth.

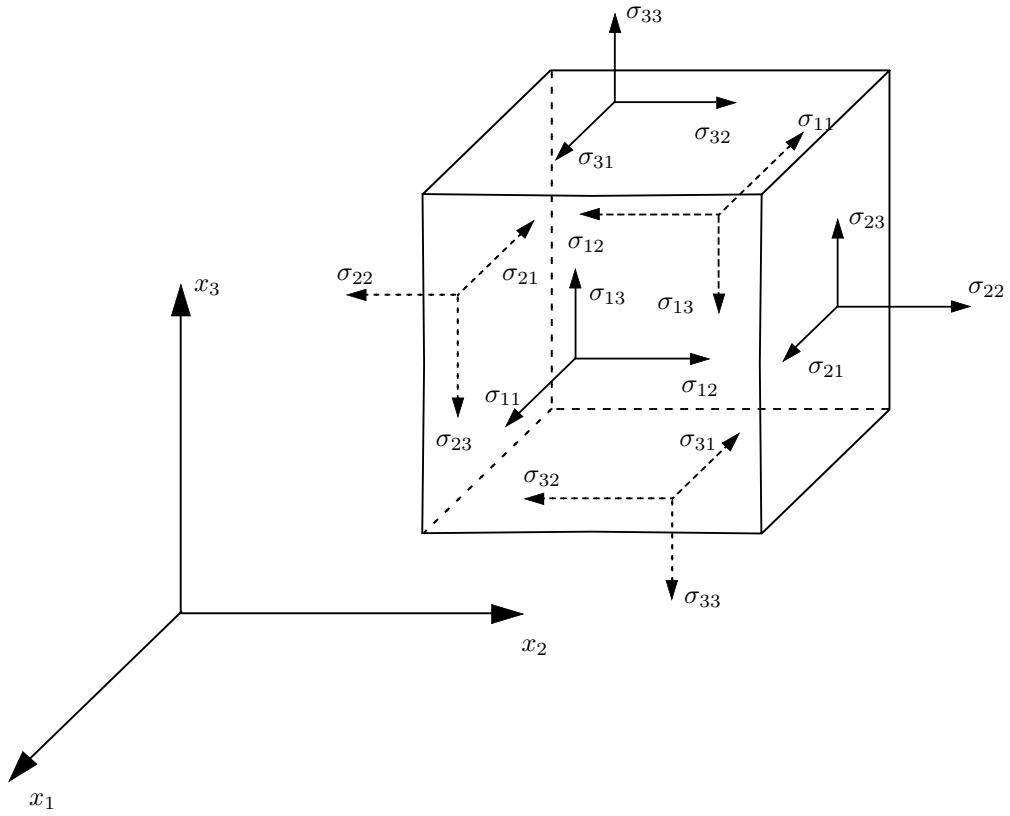

Figure 1: Stress tensor components

Another essential concept is that of the material derivative - present in the Navier-Stokes equations, it can defined for any scalar, vector, or tensor:

$$\frac{D}{Dt} := \partial_t + \mathbf{u} \cdot \nabla$$

where $\mathbf{u} = \mathbf{u}(t, x, y, z)$ is the velocity vector. Intuitively, the material derivative describes the rate of change of some physical quantity along particle paths [4].

Let us now proceed to look more formally at the different types of fluids we will be working with.

1.1 Fluid Types

Newtonian Fluids A Newtonian fluid is one that has a constant viscosity: $\eta(\dot{\gamma}) = \mu$. They display a linear relation between shear rate and shear stress:

$$\sigma_{xy} = \mu\dot{\gamma}. \tag{1.1.1}$$

Whenever we consider a constant viscosity, we shall denote it hereafter with μ. As one would suspect, Isaac Newton was the first to formulate this relation for a class of fluids, hence they are known as Newtonian.

Some examples of Newtonian fluids include: organic solvents, water and honey, in increasing order of viscosity. Despite their apparent differences, they are all classed in the same way due to the same manner in which they respond to stress.

When we can assume a fluid to be Newtonian, or at least Newtonian under conditions imposed on our particular flow, we can attempt to solve for its velocity using the Navier-Stokes equations (section 1.2).

Non-Newtonian Fluids As its name suggests, any fluid which is not Newtonian falls under the umbrella term 'non-Newtonian'. These can range vastly, from ketchup and toothpaste to glass and gels. In this report we mostly focus on viscoelastic fluids, which we consider using the Oldroyd-B model. By viscoelastic, we mean that the fluid has both viscous and elastic properties - it behaves to some extent similarly to both a viscous fluid such as water and an elastic solid such as rubber. These include blood and ketchup, among others.

We also separately look at a few cases of inelastic non-Newtonian fluids where the viscosity is a function of shear rate. In these cases we denote [2]

$$\eta = \eta(\dot{\gamma}). \tag{1.1.2}$$

A few common models are presented below:

Model	Viscosity $\eta(\dot{\gamma})$
power-law	$\mu\lvert\dot{\gamma}\rvert^{n-1}$
Carreau	$\eta_\infty + (\eta_0 - \eta_\infty)(1 + (\dot{\gamma}\tau_c)^2)^{(n-1)/2}$
Newtonian	μ

The τ_c that appeared above refers to some characteristic time, not to be confused with τ used in the Oldroyd-B model. These are plotted in the figure below.

Non-Newtonian fluids can also possess properties known as shear-thinning or shear-thickening[2]. A shear-thinning fluid's viscosity decreases with increasing shear rate, and a shear-thickening fluid's viscosity increases with shear rate. A famous example of a shear thickening fluid is cornstarch mixed with water. Examples of shear thinning fluids include toothpaste, paint and blood. Indeed, when we squeeze toothpaste, a pressure gradient is applied such that we induce a Poiseuille flow, with higher shear rates and thus lower viscosity close to the walls of the tube, serving as lubrication; while the toothpaste closer to the center of the tube retains high viscosity, which is why it often exits the tube in a cylindrical shape, and does not flow under the low shear of gravity.

We observe that a power-law fluid is shear-thickening when $n > 1$ and shear-thinning when $n < 1$; a Carreau fluid is shear-thickening when $\eta_0 < \eta_\infty$ and shear-thinning when $\eta_0 > \eta_\infty$.[2]

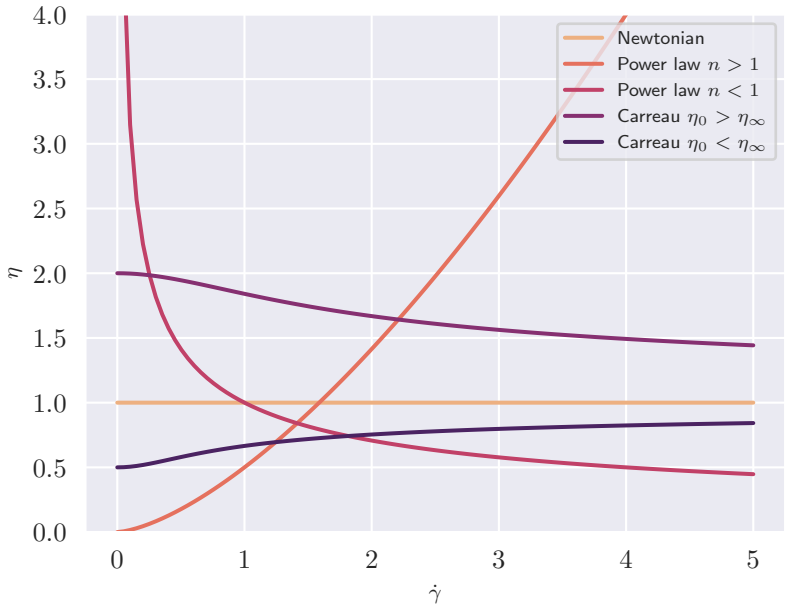

Figure 2: Viscosity vs shear rate for different fluid models

1.2 Navier-Stokes Equations

As discussed in the introduction, A motif of this report is solving the Navier-Stokes equations under various conditions imposed to find the velocity fields. We use these equations to model the flow of both Newtonian and non-Newtonian viscous fluids, treating η as constant and non-constant in each case respectively. The Navier-Stokes equations for an incompressible fluid consist of two equations, which are often presented in the following form:

$$\nabla \cdot \mathbf{u} = 0 \tag{1.2.1}$$

$$\rho \frac{D\mathbf{u}}{Dt} = -\nabla p + \eta \nabla^2 \mathbf{u} + F_{\text{ext}} \tag{1.2.2}$$

where F_{ext} denotes the sum of external forces acting on the fluid, which is often simply ρg, the force due to gravity on a unit volume of fluid. In some other occasions, it can be buoyancy or the Coriolis force [4]. The above equations are known as the continuity equation and the momentum equation respectively; the former corresponds to mass conservation and the latter to Newton's second law. $-\nabla p$ is the negative pressure gradient, corresponding to the force on a fluid element due to change in pressure, and $\eta \nabla^2 \mathbf{u}$ describes the effect of friction. In the following sections it will be useful for us to restate the momentum equation as follows (where we ignore any external forces):

$$\rho \frac{D\mathbf{u}}{Dt} = \nabla \cdot \boldsymbol{\sigma} \tag{1.2.3}$$

$$\boldsymbol{\sigma} = -p\mathbf{I} + \eta(\boldsymbol{\nabla}\mathbf{u} + (\boldsymbol{\nabla}\mathbf{u})^T) \tag{1.2.4}$$

with $\boldsymbol{\sigma}$ being the stress tensor discussed previously. We omit the derivation of the form of $\boldsymbol{\sigma}$, but details can be found in [5, Sonin]. Here, $\boldsymbol{\nabla}\mathbf{u}$ is a tensor derivative, the *velocity gradient tensor* and $\nabla \cdot \boldsymbol{\sigma}$ is the divergence of the stress tensor. For sections 2 and 3, $\boldsymbol{\nabla}\mathbf{u}$ can be simply treated as the transpose of the Jacobian of $\mathbf{u}$. We will return to this in section 4, where we discuss blood flow. The divergence of the stress tensor vector quantity, where in Cartesian coordinates the i-th component equals the divergence of the i-th column of $\boldsymbol{\sigma}$. Informally, (still in Cartesian coordinates) this can be written

$$\nabla \cdot \boldsymbol{\sigma} = \begin{pmatrix} \partial_x & \partial_y \end{pmatrix} \begin{pmatrix} \sigma_{xx} & \sigma_{xy} \\ \sigma_{yx} & \sigma_{yy} \end{pmatrix} \tag{1.2.5}$$

Furthermore, we can verify that in the two dimensional case in Cartesian coordinates, given (1.1.1) holds, this exactly agrees with (1.1.2). Indeed,

$$\boldsymbol{\sigma} = \begin{pmatrix} -p + 2\eta\partial_x u_x & \eta\left(\partial_x u_y + \partial_y u_y\right) \\ \eta\left(\partial_x u_y + \partial_y u_x\right) & -p + 2\eta\partial_x u_y \end{pmatrix} \tag{1.2.6}$$

and so

$$\begin{aligned} \nabla \cdot \boldsymbol{\sigma} &= \begin{pmatrix} -\partial_x p + \eta\left(\partial_{xx} u_x + \partial_{yy} u_x\right) + \eta\left(\partial_{xx} u_x + \partial_{xy} u_y\right) \\ -\partial_y p + \eta\left(\partial_{xx} u_y + \partial_{yy} u_y\right) + \eta\left(\partial_{yy} u_y + \partial_{xy} u_x\right) \end{pmatrix} \\ &= \begin{pmatrix} -\partial_x p + \eta\left(\partial_{xx} u_x + \partial_{yy} u_x\right) \\ -\partial_y p + \eta\left(\partial_{xx} u_y + \partial_{yy} u_y\right) \end{pmatrix} \\ &= -\nabla p + \eta \nabla^2 \mathbf{u} \end{aligned}$$

where we have used (1.1.1) to simplify. We claimed that (1.2.3) is Newton's second law ($ma = F$). While it is evident that the LHS can be obtained by dividing the volume, the RHS might not be obvious. Consider a volume of fluid as in Figure 1, and denote $F_S = (F_x, F_y, F_z)^T$ as the surface forces. Then

$$F_S = \begin{pmatrix} (\sigma_{xx} + \partial_x \sigma_{xx}\Delta x - \sigma_{xx})\Delta y \Delta z + (\sigma_{yx} + \partial_y \sigma_{yx}\Delta y - \sigma_{yx})\Delta x \Delta z + (\sigma_{zx} + \partial_z \sigma_{zx}\Delta z - \sigma_{zx})\Delta x \Delta y \\ (\sigma_{xy} + \partial_x \sigma_{xy}\Delta x - \sigma_{xy})\Delta y \Delta z + (\sigma_{yy} + \partial_y \sigma_{yy}\Delta y - \sigma_{yy})\Delta x \Delta z + (\sigma_{zy} + \partial_z \sigma_{zy}\Delta z - \sigma_{zy})\Delta x \Delta y \\ (\sigma_{xz} + \partial_x \sigma_{xz}\Delta x - \sigma_{xz})\Delta y \Delta z + (\sigma_{yz} + \partial_y \sigma_{yz}\Delta y - \sigma_{yz})\Delta x \Delta z + (\sigma_{zz} + \partial_z \sigma_{zz}\Delta z - \sigma_{zz})\Delta x \Delta y \end{pmatrix} \text{ [5]}$$

$$= \begin{pmatrix} (\partial_x \sigma_{xx} + \partial_y \sigma_{yx} + \partial_z \sigma_{zx})\Delta x \Delta y \Delta z \\ (\partial_x \sigma_{xy} + \partial_y \sigma_{yy} + \partial_z \sigma_{zy})\Delta x \Delta y \Delta z \\ (\partial_x \sigma_{xz} + \partial_y \sigma_{yz} + \partial_z \sigma_{zz})\Delta x \Delta y \Delta z \end{pmatrix}$$

$$= (\nabla \cdot \boldsymbol{\sigma})\Delta x \Delta y \Delta z$$

Therefore, we get $\nabla \cdot \boldsymbol{\sigma}$ is the net surface force per unit volume as expected.

1.3 The Oldroyd-B Model [1]

The Oldroyd-B equations model viscoelastic fluids, where elasticity is introduced by the presence of polymers suspended in a viscous solvent (where we assume to be Newtonian). We have the four governing equations

$$\nabla \cdot \mathbf{u} = 0 \tag{1.3.1}$$

$$\rho \frac{D\mathbf{u}}{Dt} = \nabla \cdot \boldsymbol{\sigma} \tag{1.3.2}$$

$$\boldsymbol{\sigma} = -p\mathbf{I} + \eta(\boldsymbol{\nabla}\mathbf{u} + (\boldsymbol{\nabla}\mathbf{u})^T) + G\mathbf{A} \tag{1.3.3}$$

$$\frac{D\mathbf{A}}{Dt} - \mathbf{A}(\boldsymbol{\nabla}\mathbf{u}) - (\boldsymbol{\nabla}\mathbf{u})^T\mathbf{A} = -\frac{1}{\tau}(\mathbf{A} - \mathbf{I}). \tag{1.3.4}$$

The Oldroyd-B model can be seen as an extension of the Navier-Stokes equations we used to model viscous fluids: we introduce an extra polymer stress term $G\mathbf{A}$ into the stress tensor $\boldsymbol{\sigma}$ to model polymeric behaviour, where $\mathbf{A}$ is known as the *conformation tensor* and is symmetric. We model polymers as pairs of spheres connected by springs, henceforth identified as "dumbbells"[6].

$$G = \frac{3\pi\eta a m}{2\tau}$$

is a material constant:

- a denotes the average size of a random polymer coil
- m is the number of dumbbells per unit volume
- τ is the time for a typical dumbbell to return to a relaxed state following deformation by the flow.

We do not delve into the details of the derivation of this model; however, one can be found in [6]. In order to solve for the velocity field when using the Oldroyd-B model, we will broadly need to:

1. Solve for relevant entries A_{ij} of $\mathbf{A}$ from a system of equations
2. Substitute into the stress tensor and hence the momentum equation
3. Solve the momentum equation for the velocity field

although this exact sequence is not always possible. In the forthcoming sections we often consider $\mathbf{u} = \mathbf{u}(t, y)$ to be independent of x (in a 2D flow), and that u_y, the y-component of the velocity, is zero. It will be useful for us to simplify in particular (1.3.4), which will provide us with the system of partial differential equations we need in step 1. Due to the variety of cases we will consider, we do not yet restrict ourselves on the dependencies of $\mathbf{A}$ (so $\mathbf{A} = \mathbf{A}(t, x, y)$). Expanding (1.3.4),

$$\partial_t\mathbf{A} + u_x\partial_x\mathbf{A} - \mathbf{A}\begin{pmatrix} 0 & 0 \\ \partial_y u_x & 0 \end{pmatrix} - \begin{pmatrix} 0 & \partial_y u_x \\ 0 & 0 \end{pmatrix}\mathbf{A} = -\frac{1}{\tau}\begin{pmatrix} A_{xx} - 1 & A_{xy} \\ A_{xy} & A_{yy} - 1 \end{pmatrix}$$

and we can read off the three conformation tensor equations for A_{xx}, A_{xy} and A_{yy}:

$$\begin{cases} \partial_t A_{xx} + u_x\partial_x A_{xx} - 2A_{xy}\partial_y u_x = -\frac{1}{\tau}(A_{xx} - 1) \\ \partial_t A_{xy} + u_x\partial_x A_{xy} - A_{yy}\partial_y u_x = -\frac{1}{\tau}A_{xy} \\ \partial_t A_{yy} + u_x\partial_x A_{yy} = -\frac{1}{\tau}(A_{yy} - 1) \end{cases} \tag{1.3.5}$$

Some examples of viscoelastic fluids which can be modelled using these Oldroyd-B equations include: blood, paints, and any other fluid that is made from a polymer mixed into a solvent.

2 Canonical Rectilinear Shearing Flows

We examine archetypal rectilinear shearing flows - that of the Couette flow and Poiseuille flow, in the cases of a viscous fluid and a viscoelastic fluid.

2.1 Couette - Newtonian Case

In this subsection, we will solve for the velocity field in a Couette flow for a Newtonian fluid. This is a steady flow between 2 plates, one or both of which are moving at a constant velocity. The motion of the fluid is driven purely by the motion of the plates, so there exists no pressure gradient, and there are no external forces acting on the fluid. By nature of this physical configuration - no conditions vary in x or t, as the flow is steady - we deduce that there is no x or t-dependence in the velocity field; i.e. $\mathbf{u} = \mathbf{u}(y)$.

First consider a plane Couette flow where the fixed lower plate is situated at $y = 0$ and the upper plate at $y = H$ has a velocity of U_1. We deploy the Navier-Stokes equations from subsection 1.2 to solve for the velocity field.

Due to the no-slip condition, our boundary conditions are

$$\mathbf{u}(H) = \begin{pmatrix} u_x(H) \\ u_y(H) \end{pmatrix} = \begin{pmatrix} U_1 \\ 0 \end{pmatrix} \tag{2.1.1}$$

$$\mathbf{u}(0) = \mathbf{0}. \tag{2.1.2}$$

Our flow has no x-dependency, so $\partial_x u_x = 0$, and hence the continuity equation reduces to simply

$$\partial_y u_y = 0.$$

This implies that u_y is constant in y, and thus it is identically equal to its values given in the boundary conditions, meaning $u_y = 0$. This, in conjunction with our initial assumption simplify the momentum equation to

$$\partial_{yy} u_x = 0$$

which can be integrated twice to obtain

$$u_x = C_1 y + C_2 \tag{2.1.3}$$

(the second momentum equation is trivially $0 = 0$). Applying the boundary conditions, we can evaluate the constants and obtain the solution

$$\mathbf{u}(y) = \begin{pmatrix} \frac{U_1}{H} y \\ 0 \end{pmatrix}. \tag{2.1.4}$$

By tweaking the boundary conditions, we easily find the solution for a flow where both the upper and lower plates are both moving at constant velocities U_1 and U_2 respectively. Our altered boundary conditions are

$$\mathbf{u}(H) = \begin{pmatrix} U_1 \\ 0 \end{pmatrix} \quad \text{and} \quad \mathbf{u}(0) = \begin{pmatrix} U_2 \\ 0 \end{pmatrix}.$$

Since the rest of the conditions are the same, we can re-evaluate our constants in (2.1.3) to obtain

$$\mathbf{u}(y) = \begin{pmatrix} \frac{U_1 - U_2}{H} y + U_2 \\ 0 \end{pmatrix}. \tag{2.1.5}$$

2.2 Couette - Viscoelastic Case

Consider the same plane Couette setup as in the previous section, but this time with a viscoelastic rather than Newtonian fluid. Our boundary conditions remain the same

$$\mathbf{u}(H) = \begin{pmatrix} U_1 \\ 0 \end{pmatrix} \quad \text{and} \quad \mathbf{u}(0) = \begin{pmatrix} U_2 \\ 0 \end{pmatrix} \tag{2.2.1}$$

however, our governing equations will be from the Oldroyd-B model.

Our pressure gradient is 0, and the lack of x-dependency simplifies the continuity equation to $\partial_y u_y = 0$, therefore we once again deduce that $u_y = 0$. Since $\mathbf{u}$ has no x-dependency and its time derivative is 0, we expect $\mathbf{A}$ and therefore $\boldsymbol{\sigma}$ to also have no x nor t-dependency. Thus the conformation tensor equations (1.4.5) further simplify to

$$\begin{cases} 2A_{xy}\partial_y u_x = \dfrac{1}{\tau}(A_{xx} - 1) \\ A_{yy}\partial_y u_x = \dfrac{1}{\tau}A_{xy} \\ A_{yy} - 1 = 0 \end{cases} \tag{2.2.2}$$

The stress tensor with the polymer extra stress term is provided as

$$\boldsymbol{\sigma} = \begin{pmatrix} GA_{xx} & \mu\partial_y u_x + GA_{xy} \\ \mu\partial_y u_x + GA_{xy} & GA_{yy} \end{pmatrix} \tag{2.2.3}$$

and the momentum equations are hence

$$\begin{cases} 0 = \partial_x \sigma_{xx} + \partial_y \sigma_{xy} = \mu\partial_{yy} u_x + G\partial_y A_{xy} \\ 0 = \partial_x \sigma_{xy} + \partial_y \sigma_{yy} = \partial_y A_{yy} \end{cases} \tag{2.2.4}$$

From here, we solve for $\mathbf{A}$ from the system (2.2.2):

$$\begin{cases} A_{yy} = 1 \\ A_{xy} = \tau\partial_y u_x \\ A_{xx} = 2\tau^2(\partial_y u_x)^2 + 1. \end{cases} \tag{2.2.5}$$

where we observe that the solution to A_{yy} automatically satisfies the second momentum equation. Substituting the expression for A_{xy} into the first momentum equation yields

$$(\mu + G\tau)\partial_{yy} u_x = 0 \tag{2.2.6}$$

which upon solving produces the same solution (2.1.3) as the Newtonian case: $u_x = C_1 y + C_2$. Using the boundary conditions to solve for C_1 and C_2 results in the same solution

$$\mathbf{u}(y) = \begin{pmatrix} \dfrac{U_1 - U_2}{H} y + U_2 \\ 0 \end{pmatrix}. \tag{2.2.7}$$

While our velocity field is found to be the same as in the viscous case, note that our effective viscosity, defined as $\sigma_{xy}/\partial_y u_x$, is $\mu + G\tau$, whereas the viscosity for the Newtonian case was simply μ. The addition of polymers to the viscous solvent introduces elastic properties, thereby increasing the effective viscosity.

2.3 Poiseuille - Newtonian Case

In a Poiseuille flow, it will be convenient for us to reposition such that the plates are at $y = H$ and $y = -H$. These are kept fixed, and the fluid motion is driven by a constant negative pressure gradient in the x-direction: $\partial_x p_x = P_x$ and the pressure remains constant in y. As this is independent of time and constant throughout space, we again must have that $\mathbf{u} = \mathbf{u}(y)$. Our boundary conditions are therefore

$$\mathbf{u}(t, H) = \mathbf{u}(t, -H) = \mathbf{0}. \tag{2.3.1}$$

We are working with a Newtonian fluid, so we use the Navier-Stokes equations from section 1.3. The continuity equation is, as before, reduced to

$$\partial_y u_y = 0$$

which again implies $u_y = 0$, and our momentum equation becomes (second momentum equation is 0=0)

$$P_x = \mu \partial_{yy} u_x \tag{2.3.2}$$

Integrating (2.3.2) twice gives

$$u_x = \frac{P_x}{2\mu} y^2 + C_1 y + C_2, \tag{2.3.3}$$

and applying the boundary conditions returns the solution

$$\mathbf{u}(y) = \begin{pmatrix} \frac{P_x}{2\mu}(y^2 - H^2) \\ 0 \end{pmatrix}. \tag{2.3.4}$$

This is a particularly simple case, but will prove to be useful in comparisons later on.

2.4 Poiseuille - Viscoelastic Case

The assumptions and conditions are largely the same as the viscoelastic Couette case and the Newtonian Poiseuille case. This means the simplifications to the Oldyroyd-B equations are almost identical to the viscoelastic Couette flow - the only difference is that $\boldsymbol{\sigma}$ has an x-dependency since $\partial_x p = P_x$, a constant instead of 0. Therefore we have the simplification $u_y = 0$ as well as our previous solutions for entries of $\mathbf{A}$ (2.2.5):

$$\begin{cases} A_{yy} = 1 \\ A_{xy} = \tau \partial_y u_x \\ A_{xx} = 2\tau^2 (\partial_y u_x)^2 + 1. \end{cases} \tag{2.4.1}$$

though now the momentum equations simplify to

$$\begin{cases} 0 = \partial_x \sigma_{xx} + \partial_y \sigma_{xy} = -P_x + \mu \partial_{yy} u_x + G \partial_y A_{xy} \\ 0 = \partial_x \sigma_{xy} + \partial_y \sigma_{yy} = \partial_y A_{yy} \end{cases} \tag{2.4.2}$$

since

$$\boldsymbol{\sigma} = \begin{pmatrix} -p + GA_{xx} & \mu \partial_y u_x + GA_{xy} \\ \mu \partial_y u_x + GA_{xy} & -p + GA_{yy} \end{pmatrix}. \tag{2.4.3}$$

Substituting A_{xy} and rearranging the first momentum equation,

$$-P_x + (\mu + G\tau)\partial_{yy}u_x = 0 \implies \partial_{yy}u_x = \frac{P_x}{\mu + G\tau}. \tag{2.4.4}$$

Integrating twice reveals

$$u_x = \frac{P_x}{2(\mu + G\tau)}y^2 + C_1 y + C_2 \tag{2.4.5}$$

and applying the boundary conditions results in the solution

$$\mathbf{u}(y) = \begin{pmatrix} \frac{P_x}{2(\mu + G\tau)}(y^2 - H^2) \\ 0 \end{pmatrix}. \tag{2.4.6}$$

As with the Couette flow, the solutions for the Newtonian and the viscoelastic cases are similar, with a key difference in the effective viscosity: μ for the Newtonian case, and $\mu + G\tau$ for the viscoelastic case.

2.5 Poiseuille - Power-law Case

Now we consider a different fluid model: the power-law model. This is a non-Newtonian, viscous fluid, meaning we still apply the Navier-Stokes momentum equations, but this time, our viscosity is non-constant. We have the shear rate dependent viscosity

$$\eta(\dot{\gamma}) = \mu|\dot{\gamma}|^{n-1}$$

Since the flow is only driven by a constant positive pressure gradient in the x-direction, i.e. no y and time dependency, we should expect $u_y = 0$ and $\partial_t \mathbf{u} = 0$. Thus

$$\partial_x p = \partial_y(\eta(\dot{\gamma})\partial_y u_x) \tag{2.5.1}$$

We have boundary conditions $\mathbf{u}(H,t) = \mathbf{0}$ and $\mathbf{u}(-H,t) = \mathbf{0}$ given by the no-slip assumption. Additionally, due the symmetry of the problem, we have $\dot{\gamma}(y=0) = 0$ [7]
Consider $H > y > 0$ and $\partial_x p > 0$ so that $\dot{\gamma} > 0$:

$$\partial_x p = \mu\partial_y((\partial_y u_x)^n)$$

Rearranging, we get

$$\partial_y u = (\frac{1}{\mu}\partial_x p y + C_1)^{\frac{1}{n}}.$$

By $\dot{\gamma}(y=0) = 0$, we get $C_1 = 0$, and using $u_x(H,t) = 0$,

$$u_x(y) = \frac{n}{n+1}(\frac{1}{\mu}\partial_x p)^{\frac{1}{n}}(y^{\frac{n+1}{n}} - H^{\frac{n+1}{n}}).$$

For $-H < y < 0$ and $\partial_x p > 0$

$$u_x(y) = \frac{n}{n+1}(\frac{1}{\mu}\partial_x p)^{\frac{1}{n}}((-y)^{\frac{n+1}{n}} - H^{\frac{n+1}{n}})$$

hence, for $\partial_x p > 0$

$$u_x(y) = \frac{n}{n+1}(\frac{1}{\mu}\partial_x p)^{\frac{1}{n}}(|y|^{\frac{n+1}{n}} - H^{\frac{n+1}{n}}). \tag{2.5.2}$$

We get $u_x(y)$ for $\partial_x p < 0$ by symmetry

$$u_x(y) = -\frac{n}{n+1}(-\frac{1}{\mu}\partial_x p)^{\frac{1}{n}}(|y|^{\frac{n+1}{n}} - H^{\frac{n+1}{n}}) \tag{2.5.3}$$

Combining all the cases, we get

$$u_x(y) = \frac{\partial_x p}{|\partial_x p|}\frac{n}{n+1}(\frac{1}{\mu}|\partial_x p|)^{\frac{1}{n}}(|y|^{\frac{n+1}{n}} - H^{\frac{n+1}{n}}) \tag{2.5.4}$$

2.6 Plots, Comparisons and Analysis

We omit the plots for the Couette flow since the flow profiles for both cases are identical and linear. We will include different cases for the Poiseuille flow, see Figure 3, where we fixed $\mu = 1$ and $H = 1$, for the left column, we have

- top: $n = 0.5$ (shear-thinning) with various pressure gradients
- middle: $n = 1$ (Newtonian) with various pressure gradients
- bottom: $n = 2$ (shear-thickening) with various pressure gradients

For the right column, we have

- top: $\partial_x p = -1$ with various n
- middle: $\partial_x p = -5$ with various n
- bottom: $\partial_x p = -10$ with various n

From the left column of Figure 3, we observe that the flow is more pointed for a shear-thickening fluid (bottom: $n = 2$) and more like a plug flow in the middle for a shear-thinning fluid (top: $n = 0.5$). The middle one is the Newtonian case where $n = 1$. We also notice that for $\partial_x p = -1$ (top right), u_x increases as n increases, which is not the case for the other two plots.
To investigate this and for simplicity, we set $\mu = 1$, $H = 1$, $\partial_x p < 0$ and consider

$$u_x(0) = \frac{n}{n+1}(-\partial_x p)^{\frac{1}{n}}$$

Differentiating, we find that the stationary point of $u_x(0)$ is greater than zero only when $1 < -\partial_x p < e$, which means that the velocity will first decrease and then increase as n increases. For $-\partial_x p > e$, $u_x(0)$ is strictly monotonically decreasing for $n > 0$; for $-\partial_x p < 1$, $u_x(0)$ is strictly monotonically increasing for $n > 0$. This explains why we have a different relationship between u_x and n with varying pressure gradient.
For $n < 1$ in the power-law model, $\eta(\dot{\gamma}) = \mu|\dot{\gamma}|^{n-1}$, $\eta \to \infty$ as $\dot{\gamma} \to 0$, which is not practical. To overcome this restriction, the Carreau model is used, which is mentioned in subsection 3.3 in greater detail.

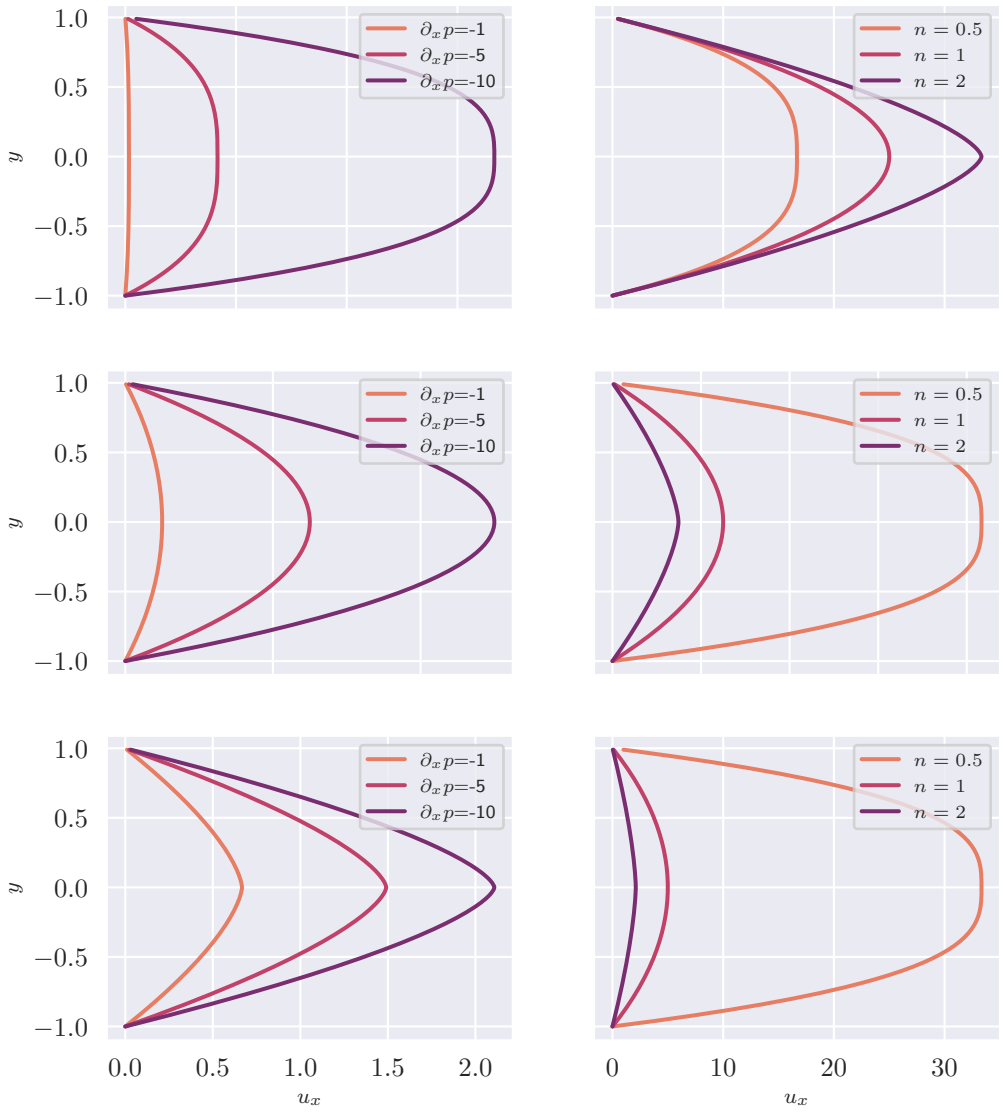

Figure 3: Velocity profile of Poiseuille flow with power-law

3 Harmonic Oscillation

We now proceed to direct our attention towards the problem where one or both plates undergo simple harmonic motion. That is, the plate(s) move back and forth horizontally in a sinusoidal motion, which will induce a flow of the fluid between them.

3.1 Newtonian Case

We first consider the problem for a Newtonian fluid. Let us start with the case where only the top plate is in motion and the bottom plate remains at rest, so we have the boundary conditions

$$\mathbf{u}(t,H) = \begin{pmatrix} u_x(t,H) \\ u_y(t,H) \end{pmatrix} = \begin{pmatrix} U_1 \cos(\omega_1 t) \\ 0 \end{pmatrix} \tag{3.1.1}$$

$$\mathbf{u}(t,0) = \mathbf{0} \tag{3.1.2}$$

where again the plates are separated by H, with U_1 being the amplitude of oscillation. We set the pressure to be constant so that the fluid is driven solely by the movement of the plate(s). No additional x-dependency has been introduced in our physical configuration, therefore we expect our solution to only depend on t and y. Hence the continuity equation simplifies to

$$\partial_y u_y = 0. \tag{3.1.3}$$

This shows u_y is some arbitrary function of t, so the boundary conditions imply that this is identically zero. Hence in this case the momentum equation becomes

$$\partial_t u_x = \nu \partial_{yy} u_x \tag{3.1.4}$$

where we have denoted

$$\frac{\mu}{\rho} = \nu.$$

with μ being the constant viscosity of the Newtonian fluid (the equation for the y-component is trivially $0 = 0$).

We solve over the domain

$$t \in \mathbb{R} \qquad 0 \leq y \leq H$$

so we can proceed with a Fourier transform in t to obtain

$$i\omega \hat{u}_x = \nu \partial_{yy} \hat{u}_x, \qquad \hat{u}_x = \hat{u}_x(\omega, y). \tag{3.1.5}$$

Treating this as a second order ODE, we find the roots of the characteristic equation are

$$\lambda = \pm e^{i\pi/4} \sqrt{\frac{\omega}{\nu}} = \pm(1+i)\sqrt{\frac{\omega}{2\nu}}$$

and so the transformed solution can be written in the general form

$$\hat{u}_x = A(\omega)\cosh\left((1+i)\sqrt{\frac{\omega}{2\nu}}y\right) + B(\omega)\sinh\left((1+i)\sqrt{\frac{\omega}{2\nu}}y\right). \tag{3.1.6}$$

Transforming the boundary conditions (3.1.1) and (3.1.2) gives

$$\hat{u}_x(\omega, H) = \mathcal{F}\{U_1 \cos(\omega_1 t)\} = U_1 \pi(\delta(\omega - \omega_1) + \delta(\omega + \omega_1)) \tag{3.1.7}$$

$$\hat{u}_x(\omega, 0) = 0 \tag{3.1.8}$$

and upon plugging into (3.1.6) reveals

$$A(\omega) = 0 \tag{3.1.9}$$

$$B(\omega) = \frac{U_1 \pi(\delta(\omega - \omega_1) + \delta(\omega + \omega_1))}{\sinh(\lambda(\omega)H)} \tag{3.1.10}$$

where we have introduced

$$\lambda(\omega) = (1+i)\sqrt{\frac{\omega}{2\nu}} \tag{3.1.11}$$

for sake of simplicity. It will be helpful to require at this point that

$$\lambda(-\omega) = (1-i)\sqrt{\frac{\omega}{2\nu}} = \overline{\lambda(\omega)}. \tag{3.1.12}$$

which is appropriate as $\lambda(\omega)^2 = \lambda(-\omega)^2$ is maintained. We are ready to take the inverse Fourier transform to recover u_x. This is

$$\begin{aligned}
u_x(t,y) &= \frac{1}{2\pi}\int_{\mathbb{R}} \hat{u}_x(\omega, y) e^{i\omega t} d\omega \\
&= \frac{U_1}{2}\int_{\mathbb{R}} (\delta(\omega-\omega_1) + \delta(\omega+\omega_1)) \frac{\sinh(\lambda(\omega)y)}{\sinh(\lambda(\omega)H)} e^{i\omega t} d\omega \\
&= \frac{U_1}{2}\left(\frac{\sinh(\lambda(\omega_1)y)}{\sinh(\lambda(\omega_1)H)} e^{i\omega_1 t} + \frac{\sinh(\lambda(-\omega_1)y)}{\sinh(\lambda(-\omega_1)H)} e^{-i\omega_1 t} \right) \\
&\overset{(3.1.12)}{=} U_1 \mathrm{Re}\left\{ \frac{\sinh(\lambda(\omega_1)y)}{\sinh(\lambda(\omega_1)H)} e^{i\omega_1 t} \right\}
\end{aligned} \tag{3.1.13}$$

where in the last line we used the fact that $\sinh(\overline{z}) = \overline{\sinh(z)}$, and the sifting property of the Dirac delta function is used in the penultimate line.

We would like to find the solution for a more general case - where both the top and bottom plates are in oscillation, possibly with a phase difference. Without loss of generality, we can assume that the bottom plate oscillates without phase shift, and that the top plate oscillates with a phase difference ϕ. That is, to solve with boundary conditions

$$\mathbf{u}(t, H) = \begin{pmatrix} U_1 \cos(\omega_1 t + \phi) \\ 0 \end{pmatrix} \tag{3.1.14}$$

$$\mathbf{u}(t, 0) = \begin{pmatrix} U_2 \cos(\omega_2 t) \\ 0 \end{pmatrix} \tag{3.1.15}$$

To this end, we address two obstacles:

1. Modify our solution (3.1.13) to include phase shift ϕ
2. Find the solution to the initial value problem where only the bottom plate is oscillating and the top plate is at rest

Once these are achieved, we may simply employ the principle of superposition to deduce the desired result. For the first point, we consider the Fourier transform of $U_1 \cos(\omega_1 t + \phi)$:

$$\begin{aligned}\mathcal{F}\{U_1 \cos(\omega_1 t + \phi)\} &= \frac{U_1}{2}\mathcal{F}\{e^{i(\omega_1 t+\phi)} + e^{-i(\omega_1 t+\phi)}\} \\ &= \frac{U_1}{2}(e^{i\phi}\mathcal{F}\{e^{i\omega_1 t}\} + e^{-i\phi}\mathcal{F}\{e^{-i\omega_1 t}\}) \\ &= U_1\pi(e^{i\phi}\delta(\omega-\omega_1) + e^{-i\phi}\delta(\omega+\omega_1)) \end{aligned} \tag{3.1.16}$$

And so it is clear that (3.1.10) will be modified accordingly, thus yielding

$$u_x(t,y) = U_1 \mathrm{Re}\left\{\frac{\sinh(\lambda(\omega_1)y)}{\sinh(\lambda(\omega_1)H)} e^{i(\omega_1 t+\phi)}\right\}. \tag{3.1.17}$$

For the second point, we need to solve for $A(\omega)$ and $B(\omega)$ using the boundary conditions (3.1.15) and

$$\mathbf{u}(t,H) = \mathbf{0}. \tag{3.1.18}$$

These have, for u_x, transformations

$$\hat{u}_x(\omega, H) = 0 \tag{3.1.19}$$

$$\hat{u}_x(\omega,0) = \mathcal{F}\{U_2\cos(\omega_2 t)\} = U_2\pi(\delta(\omega-\omega_2)+\delta(\omega+\omega_2)) \tag{3.1.20}$$

and plugging into (3.1.6) gives

$$A(\omega) = \hat{u}_x(\omega,0) \tag{3.1.21}$$

$$B(\omega) = \hat{u}_x(\omega,0)\left(-\frac{\cosh(\lambda(\omega)H)}{\sinh(\lambda(\omega)H)}\right) \tag{3.1.22}$$

from which we recover, similar to the previous case,

$$\begin{aligned} u_x(t,y) &= \frac{1}{2\pi}\int_{\mathbb{R}} \hat{u}_x(\omega,y)e^{i\omega t}d\omega \\ &= \frac{U_2}{2}\int_{\mathbb{R}} (\delta(\omega-\omega_2)+\delta(\omega+\omega_2))\left(\cosh(\lambda(\omega)y) - \frac{\cosh(\lambda(\omega)H)}{\sinh(\lambda(\omega)H)}\sinh(\lambda(\omega)y)\right)e^{i\omega t}d\omega \\ &\overset{(3.1.12)}{=} U_2\mathrm{Re}\left\{\left(\cosh(\lambda(\omega_2)y) - \frac{\cosh(\lambda(\omega_2)H)}{\sinh(\lambda(\omega_2)H)}\sinh(\lambda(\omega_2)y)\right)e^{i\omega_2 t}\right\} \end{aligned} \tag{3.1.23}$$

Finally, the solution to the problem with boundary conditions (3.1.14) and (3.1.15) is just the sum of (3.1.17) and (3.1.23), as both solve the momentum and mass conservation equations and the sum satisfies the boundary conditions. In particular, if $U_1 = U_2$, $\omega_1 = \omega_2$ and $\phi = 0$, we have that the plates are synchronised in oscillation, and the solution can be expressed in the form

$$U_1\mathrm{Re}\left\{\left(\cosh(\lambda(\omega_1)y) + \frac{1-\cosh(\lambda(\omega_1)H)}{\sinh(\lambda(\omega_1)H)}\sinh(\lambda(\omega_1)y)\right)e^{i\omega_1 t}\right\} \tag{3.1.24}$$

We will more closely examine this case and its analogous viscoelastic solution in sections 3.3-3.4.

3.2 Viscoelastic Case

Now let us move on to the case of a viscoelastic fluid, as before modelled using the Oldroyd-B equations. We consider the same boundary conditions where both plates oscillate with potentially different frequencies with some phase difference. Again, the pressure gradient is set to zero, and we have the same mass conservation equation (3.1.3), giving $u_y = 0$. The additional term $\nabla \cdot G\mathbf{A}$ results in the following form of the momentum equation:

$$\begin{cases} \rho \partial_t u_x = \mu \partial_{yy} u_x + G \partial_y A_{xy} \\ 0 = G \partial_y A_{yy} \end{cases} \tag{3.2.1}$$

As all physical quantities are independent of x, we reason that $\mathbf{A}$ must also be independent of x. Therefore the second momentum equation gives that $A_{yy} = f(t)$ for some arbitrary f. We recall the conformation tensor equations for this case (from (1.4.5)):

$$\begin{cases} \partial_t A_{xx} - 2A_{xy}\partial_y u_x = -\dfrac{1}{\tau}\left(A_{xx} - 1\right) \\ \partial_t A_{xy} - A_{22}\partial_y u_x = -\dfrac{1}{\tau} A_{xy} \\ \partial_t A_{yy} = -\dfrac{1}{\tau}\left(A_{yy} - 1\right) \end{cases} \tag{3.2.2}$$

The third equation is separable, and upon solving yields

$$A_{yy} = 1 - F(y)e^{-t/\tau} \tag{3.2.3}$$

where F is an arbitrary function of y. By our previous discussion this must in fact be a constant. We note that there is a decay phenomenon and $\lim_{t\to\infty} A_{yy} = 1$, so for simplicity, let us require $A_{yy}|_{t=0} = 1$ so that $A_{yy} = 1 \ \ \forall t$. Then, plugging into the second equation and taking the Fourier transform in t, we acquire

$$i\omega \hat{A}_{xy} + \frac{1}{\tau}\hat{A}_{xy} = \partial_y \hat{u}_x. \tag{3.2.4}$$

We can take the partial derivative with respect to y on (3.2.4) and substitute into the Fourier transform in t of the first equation in (3.2.1) to realise

$$\rho i\omega \hat{u}_x = \mu \partial_{yy}\hat{u}_x + \frac{G}{i\omega + \frac{1}{\tau}} \partial_{yy}\hat{u}_x \tag{3.2.5}$$

at which point rearranging yields

$$\partial_{yy}\hat{u}_x = \Lambda^2 \hat{u}_x \tag{3.2.6}$$

where

$$\begin{aligned} \Lambda^2 &= \rho i\omega \left(\frac{i\omega + \frac{1}{\tau}}{\mu\omega i + \frac{\mu}{\tau} + G} \right) \\ &= \rho\omega \left(\frac{i - \tau\omega}{\mu + G\tau + \mu\tau\omega i} \right) \\ &= \rho\omega \left(\frac{(\mu - \eta)\tau\omega + (\mu\tau^2\omega^2 + \eta)i}{\eta^2 + (\mu\tau\omega)^2} \right) \qquad \text{with } \ \eta = \mu + G\tau. \end{aligned} \tag{3.2.7}$$

Similar to the Newtonian case, we note $\Lambda(\omega)^2 = \Lambda(-\omega)^2$, so we can require $\Lambda(\omega) = \overline{\Lambda(\omega)}$ for whichever choice of square root we take for Λ. Now the transformed solution has the form

$$\hat{u}_x = A(\omega)\cosh(\Lambda(\omega)y) + B(\omega)\sinh(\Lambda(\omega)y) \tag{3.2.8}$$

and the remainder of the solution is completely analogous to the Newtonian case. We thus conclude that the original solution is $u_x = u_{\text{upper}} + u_{\text{lower}}$, where

$$u_{\text{upper}} = U_1 \text{Re}\left\{\frac{\sinh(\Lambda(\omega_1)y)}{\sinh(\Lambda(\omega_1)H)} e^{i(\omega_1 t+\phi)}\right\}. \tag{3.2.9}$$

and

$$u_{\text{lower}} = U_2 \text{Re}\left\{\left(\cosh(\Lambda(\omega_2)y) - \frac{\cosh(\Lambda(\omega_2)H)}{\sinh(\Lambda(\omega_2)H)}\sinh(\Lambda(\omega_2)y)\right) e^{i\omega_2 t}\right\} \tag{3.2.10}$$

3.3 Numerical approach to Carreau Fluid Case

Recall that a Carreau fluid is a special class of non-Newtonian fluid which can behave both like a Newtonian fluid and power-law fluid depending on the value of the parameter n. Its viscosity is a function of shear rate, which we have seen in the introduction, repeated here:

$$\eta(\dot{\gamma}) = \eta_\infty + (\eta_0 - \eta_\infty)(1 + (\dot{\gamma}\tau)^2)^{\frac{n-1}{2}} \tag{3.3.1}$$

By using the result from [8, Wilson], we obtain:

$$\partial_y(\eta\dot{\gamma}) = \partial_t u \tag{3.3.2}$$

Where u is the velocity profile and takes the form $u(t, y)$. By setting $\tau = 1$ and plugging (3.3.1) into (3.3.2) we find:

$$\partial_t u = \partial_y(\eta_\infty + (\eta_0 - \eta_\infty)(1 + (\partial_y u)^2)^{\frac{n-1}{2}}\partial_y u) \tag{3.3.3}$$

Now consider the substitution:

$$v = (1 + (\partial_y u)^2)^{\frac{n-1}{2}} \tag{3.3.4}$$

We substitute v into (3.3.3) to get

$$\partial_t u = (\eta_0 - \eta_\infty)(v\partial_{yy}u + \partial_y v\partial_y u). \tag{3.3.5}$$

We will be using the Forward Euler method[9] to perform finite difference approximations for the equation above:

$$\partial_t u = \frac{u(t+\Delta t) - u(t)}{\Delta t} \tag{3.3.6}$$

$$\partial_y u = \frac{u(y+\Delta y) - u(y)}{\Delta y} \tag{3.3.7}$$

$$\partial_{yy} u = \frac{u(y+\Delta y) + u(y-\Delta y) - 2u(y)}{(\Delta y)^2} \tag{3.3.8}$$

$$\partial_y v = (n-1)(1 + (\partial_y u)^2)^{\frac{n-3}{2}}\partial_{yy}u\partial_y u \tag{3.3.9}$$

Since we know all the components appearing in both v and $\partial_y v$, we can get the full finite difference for them and the right hand side of (3.3.5).

Before introducing our full finite difference code, we firstly establish some details:

$T = 4\pi$: time-period we are investigating
$H = 5$: distance between two plates
$N = 100$: number of y-values
$Nt = 10001$: number of t-values.
$dt = T/Nt$: time difference where
$dy = H/N$: height difference

We then introduce a 2D-matrix U for the velocity profile, where each $U[i, j]$ represents the velocity at point $i\Delta y$ at time $j\Delta t$. Since we have our boundary condition $u(y = 0) = u(y = H) = sin(t)$ and our initial condition $u(t = 0) = 0$, we know $U[0, j] = U[N - 1, j] = \sin(j\Delta t)$ and $U[:, 0] = 0$. Below is the code for running through the algorithm:

```
for j in range(0, Nt - 1):
    for i in range(1, N-1):
        d2udy2 = (u[i+1,j] + u[i-1,j]-2*u[i,j])/dy**2
        dudy =(u[i+1,j] - u[i,j])/dy
        v =(1 + dudy ** 2)**((n - 1)/2)
        dvdy = (n-1) * (1 + dudy ** 2) **((n-3)/2) * d2udy2 * dudy
        u[i,j+1] = (eta_0 - eta_inf) * dt * (dvdy * dudy + v * d2udy2) + u[i,j]
```

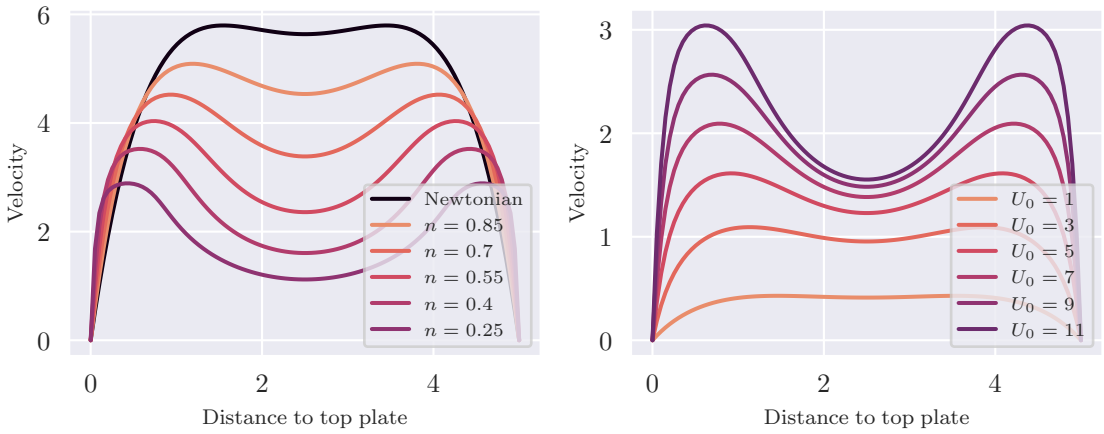

Figure 4: Velocity profile at $t = \pi$, varying n (left) and varying U_0 (right)

Here we can see there are three variables left: η_0, η_∞ and n, which are the viscosities at shear rate = 0, at shear rate = ∞, and the power, respectively. We are setting $\eta_0 = 1$ for our plots and will be changing our values of n and η_∞. The figure above shows how the fluid flow compares to Newtonian with varied n and $\eta_\infty = 0.1$ at time π (left). On the right, we vary U_0 to illustrate the shear-thinning property of the Carreau fluid. Notice that as U_0 increases,

1. The overall velocity of the fluid between the plates is higher

2. Due to increased U_0, the fluid velocity changes faster, attaining higher shear rates and becoming thinner near the plates.

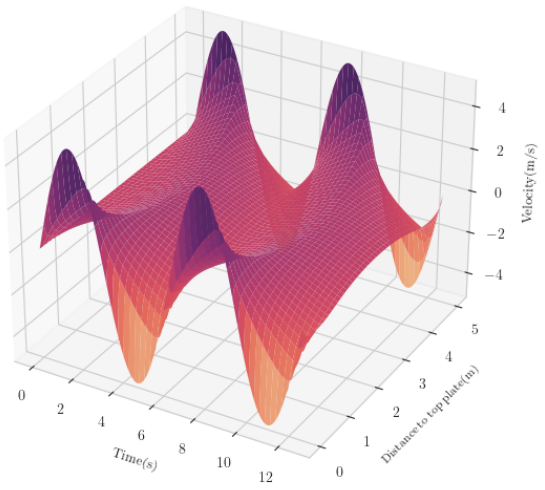

Figure 5: 3D plot of velocity profile for Carreau fluid between 2-oscillating plates

Then we set a value for n and change our values of η_∞. Below are several examples with $n = 0.7$, $n = 0.5$, $n = 0.3$ and $n = 0.1$. We also present a 3D plot showing how the velocity profile of the Carreau fluid evolves over two time periods. Note that at the boundaries they exactly follow the sinusoidal movement of the plates.

From the graphs we can see the difference between the Carreau fluid and the Newtonian fluid increases as n approaches 0. This is because n effectively controls how quickly the viscosity changes from η_0 to η_∞ as shear rate increases. The closer n is to 0, the quicker η approaches η_∞ for the same increase in $\dot{\gamma}$. We also observe that in these cases, the velocity of the plates are fixed and so as η_∞ increases, the fluid's overall velocity decreases due to this higher viscosity.

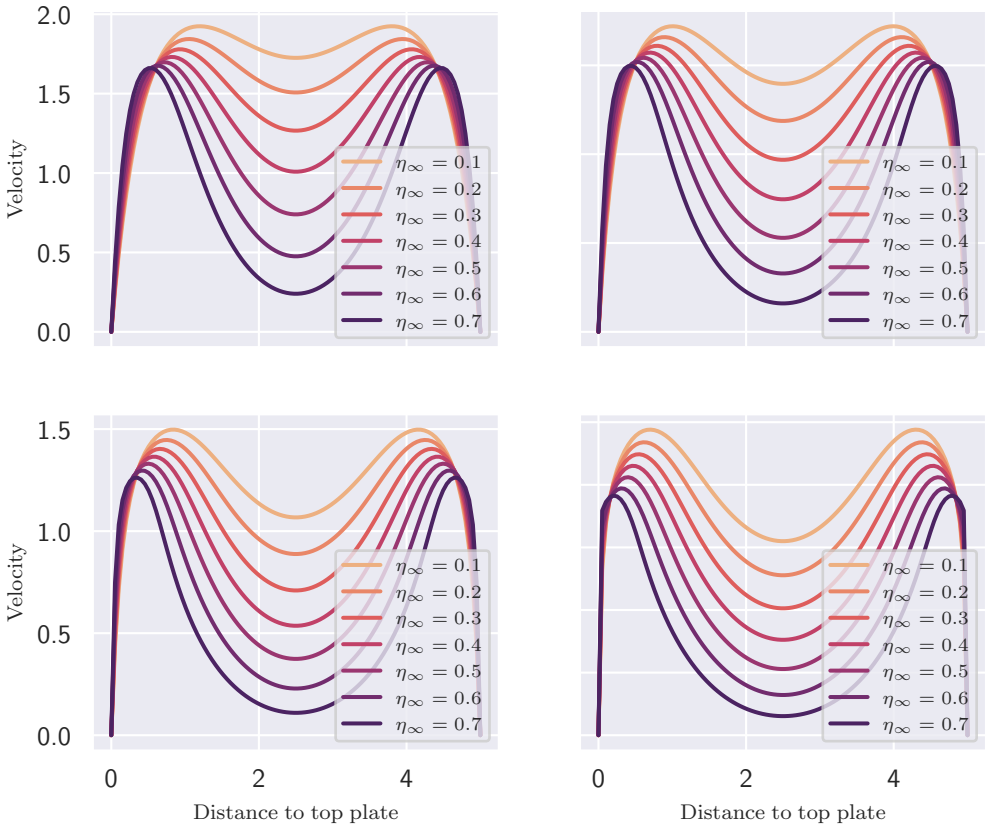

Figure 6: Velocity Profile of Carreau Fluid between 2 oscillating plates at $t = \pi$ for varying η_∞

3.4 Effective Viscosity

In this subsection we examine an interesting relationship between the Newtonian and Oldroyd-B solutions to the case of the oscillating plate problem where both plates oscillate in phase with the same amplitude. Notice that in the case of oscillating plane of Newtonian fluid, we introduced (we wrote Λ to distinguish from λ before):

$$\lambda(\omega) = (1+i)\sqrt{\frac{\omega}{2\nu}} \tag{3.4.1}$$

In a similar fashion, we introduced in the case of oscillating plane of viscoelastic fluid, we introduced:

$$\lambda(\omega) = \sqrt{\frac{\rho(i-\omega\tau)}{G\tau+\eta+\eta\omega\tau i}} \tag{3.4.2}$$

Notice that in the Newtonian case, there is a relationship between λ and the viscosity μ, as the sole difference between the solution of Newtonian and viscoelastic case is the value of λ. Hence, one may be tempted to inquire whether assigning the effective viscosity η^* of the viscoelastic fluid in a manner that equates the λ value in (3.4.1) to the λ value in (3.4.2) yields any meaningful physical implications.

$$\lambda(\omega) = (1+i)\sqrt{\frac{\omega\rho}{2\nu^*}} = \sqrt{\frac{\rho(i-\omega\tau)}{G\tau+\eta+\eta\omega\tau i}} \tag{3.4.3}$$

$$(1+i)\sqrt{\frac{\omega\rho}{2\nu^*}} = \sqrt{\frac{\rho(i-\omega\tau)}{G\tau+\eta+\eta\omega\tau i}} \tag{3.4.4}$$

$$\frac{2i}{2\eta^*} = \frac{i-\omega\tau}{G\tau+\eta+\eta\omega\tau i} \tag{3.4.5}$$

by solving we have:

$$\eta^* = \eta + \frac{G\tau}{1+(\omega\tau)^2} - \frac{G\omega\tau^2}{1+(\omega\tau)^2}i \tag{3.4.6}$$

now as discuss in previous section, we know that the relationship between τ and G, where G is the material constant defined in subsection 1.3, is that $G\tau = G^{'}$ for some constant $G^{'}$ we can further simplify η^* to the following form:

$$\eta^* = \eta + \frac{G^{'}}{1+(\omega\tau)^2} - \frac{G^{'}\omega\tau}{1+(\omega\tau)^2} \tag{3.4.7}$$

The distinction between the effective viscosity and viscosity is evident, with the former incorporating an imaginary component. Hence, it is reasonable to consider the real part of the effective viscosity as indicative of the fluid's viscous characteristics (viscous component), while the imaginary part of the viscosity signifies its elastic properties in the viscoelastic fluid (elastic component)[10]. To investigate validity of this claim, we observe various scenarios where either the viscous component or the elastic component of the viscosity holds more significance. Consider the ratio of the magnitude of elastic component and the viscous component:

$$\left|\frac{\mathrm{Re}(\eta^*)}{\mathrm{Im}(\eta^*)}\right| = \frac{\eta + \frac{G^{'}}{1+(\omega\tau)^2}}{\frac{G^{'}\omega\tau}{1+(\omega\tau)^2}} \tag{3.4.8}$$

now as $G^{'} = \frac{3\pi\eta am}{2}$, we can further simplify the ratio into a constant that depends on only the characteristics of the fluid times $\omega\tau$:

$$\left|\frac{\mathrm{Re}(\eta^*)}{\mathrm{Im}(\eta^*)}\right| = \frac{2}{3\pi am}\left(\omega\tau + \frac{1}{\omega\tau}\right) + \frac{1}{\omega\tau} \tag{3.4.9}$$

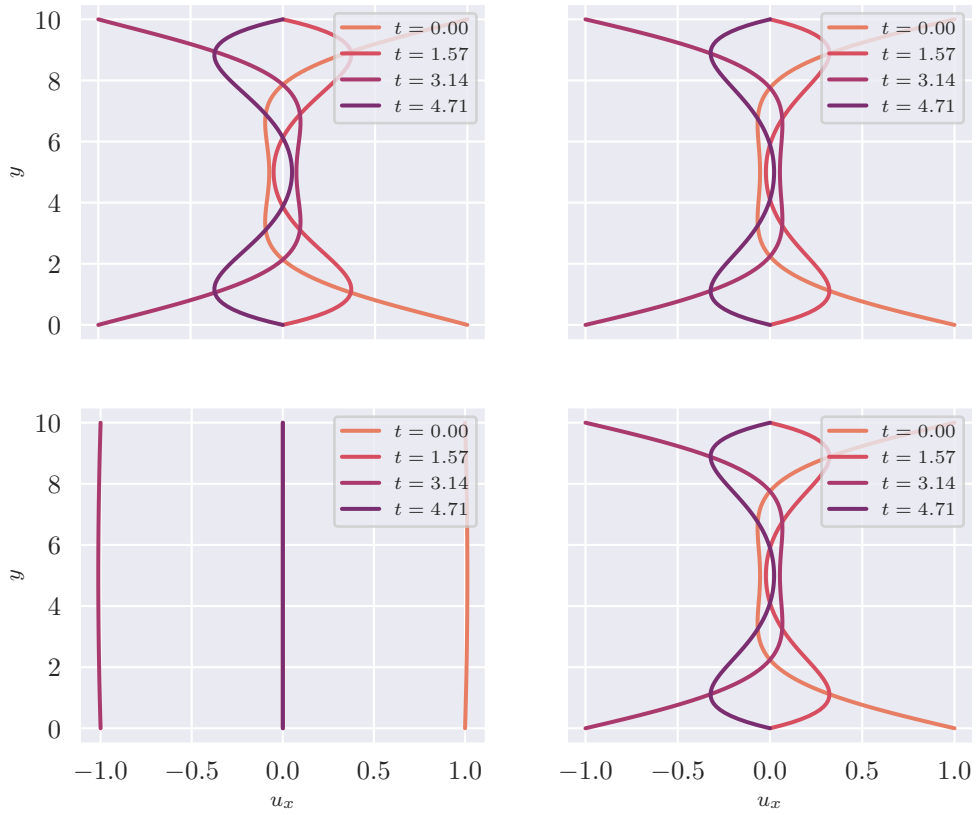

Figure 7: Velocity profiles of Oldroyd-B model and Newtonian model with real part of complex effective viscosity

Indeed, we can see that when the ratio is large (the fluid is "very viscous"), the velocity profile in such case is similar to the Newtonian case. On the contrary, when the ratio is very small, the behavior of the fluid significantly differs from that of a Newtonian fluid with the same viscosity. As observed in the plot, the velocity profile of the "very elastic" fluid appears almost as a straight line, indicating that the fluid at different heights moves together. This behavior aligns with what one would expect when placing an elastic solid between two oscillating plates. In contrast, the velocity profile of the Newtonian fluid exhibits a very wavy shape, as the liquid is free to move more freely. To further illustrate this difference, let's examine the velocity-time graph:

From the velocity-time graph for different height, we can clearly observe that the graph aligns more closely with the boundary condition for the elastic fluid, while the difference is more apparent for the Newtonian fluid. This distinction further highlights the contrasting behaviors of the two fluid types.

We observe that the term ω and τ consistently appear together in the formula for η^*, which clearly implies that the product of ω and τ has a significance in the characteristic of the viscoelastic fluid. While the formal explanation of this is a bit out of scope of this report, here is the intuitive explanation for this. From Physics, we know that:

$$T \text{ (Period of the oscillating plane)} = \frac{2\pi}{\omega} \tag{3.4.10}$$

Therefore, we have:

$$\omega\tau = 2\pi\frac{\tau}{T} \tag{3.4.11}$$

Physically, the quantity $\omega\tau$ represents the ratio of the relaxation time of the viscoelastic fluid to the period of the oscillating plates. When the relaxation time of the fluid is significantly larger than the period of the oscillating plane, it can be interpreted as the plane oscillating too rapidly for the fluid to react adequately to its movement. Consequently, the elastic characteristics of the fluid become less prominent. Conversely, when the relaxation time is more significant than the period of the oscillating plane, the elastic characteristics becomes more pronounced.

However, it is important to note that when , $\omega\tau$, tends to zero, the ratio also becomes large. This observation aligns with the fact that when τ approaches zero (note that ω cannot tend to zero as it is the essence of the oscillating fluid), a viscoelastic fluid exhibits more viscous behavior than elastic behavior(Or a Newtonian fluid is a fluid with zero relaxation time). In fact, we can find the point for $\omega\tau$ by simple differentiation, differentiating (3.4.9) we get that the ratio is minimal when $\omega\tau$ equals to:

$$\sqrt{\frac{3\pi am + 2}{2}} \tag{3.4.12}$$

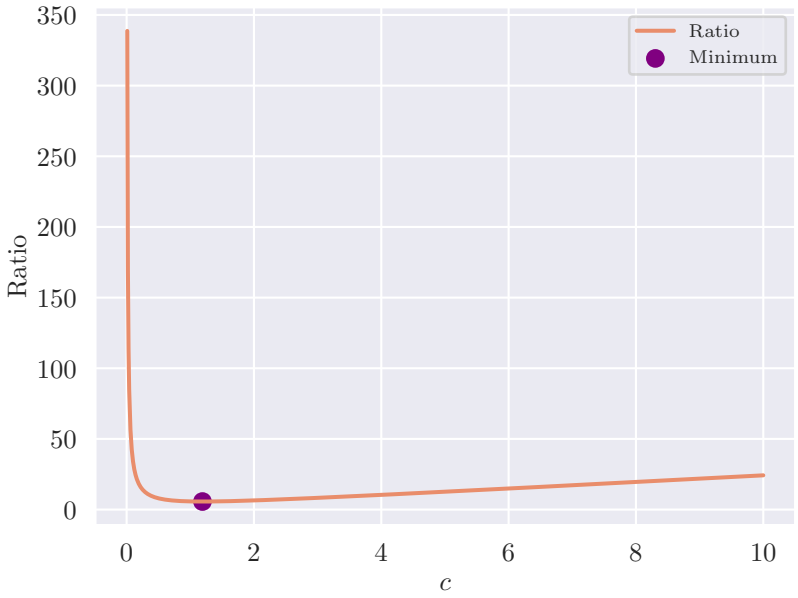

Figure 8: Ratio of real part of effective viscosity over imaginary part of viscosity vs. $c = \omega\tau$

4 Blood Flow

This section will focus on a problem with physical significance - modelling the velocity field in a blood vessel. Blood is a complex fluid exhibiting properties including shear-thinning and viscoelasticity, but can be modelled as Newtonian at high shear rates.

Naturally, understanding blood flow in various cases is decidedly important in medical applications; however, these cases can quickly become exceedingly complex to analyse analytically, and so for us to make some progress on this front, a number of simplifying assumptions must be considered[1].

The beating of the heart is assumed to be regular, which induces a periodic pressure gradient through the arteries. This means that in the arteries the flow will certainly be unsteady, and it can only be considered steady in veins and capillaries. The walls of blood vessels are viscoelastic, and in particular for large arteries the simplifying assumption that walls are rigid will break down. When we model the blood vessels as rigid cylindrical tubes, it follows that we also neglect the time it takes for the pressure to change throughout the blood vessel - i.e. that the change in pressure propagates with infinite speed (in general the speed of this propagation is much greater than the flow velocity, so that the assumption is not unreasonable). Additionally, the flow may not be laminar - though we can neglect turbulent behaviour and model the flow as laminar away from the large arteries. The effect of gravity is non-negligible in general, but we will ignore this for our simple analysis. Furthermore, we can assume blood is incompressible within blood vessels.

One might conjecture optimistically that perhaps the revolution of the solution profile for the flow between fixed plates with time-variable pressure gradient gives the solution to this problem; however,

[1] The following qualitative discussion is based on [3]

unfortunately this is not the case. Indeed, though the parallel plates solution profile will give us a sense of the solution we are after, we must ultimately resort to a cylindrical coordinate system and solve this problem in three dimensions. We begin by deriving the case of the Hagen-Poiseuille flow, which is the analog of Poiseuille flow in a cylindrical tube. This will both serve as a baseline for comparison with more complex cases and also illustrate the difference to the Poiseuille flow velocity profile. But before we can start, we must derive the corresponding equations in cylindrical polar coordinates.

4.1 Equations in Cylindrical Coordinates

Since we consider flow in the x-direction, it will be convenient to establish the coordinate system in (x, r, θ), as shown:

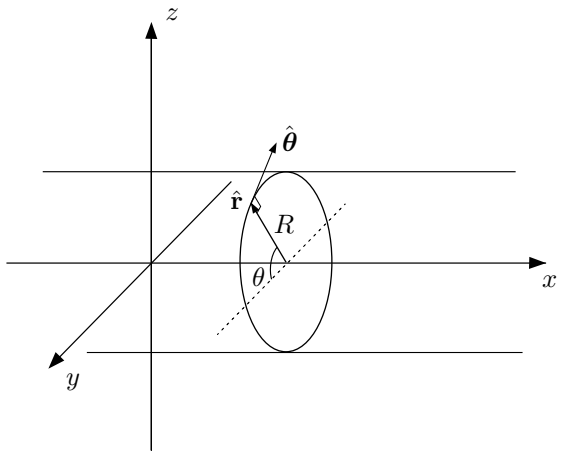

Figure 9: Cylindrical coordinates

Throughout this section, we will impose:

1. Flow is fully developed
2. No slip ($\mathbf{u}|_{r=R} = \mathbf{0}$)
3. Flow is axisymmetric (independent of θ and $\partial_r \mathbf{u}|_{r=0} = \mathbf{0}$)

As we ignore any capacity for blood vessel walls to deform (and that pressure change is instantaneous so that $\partial_x p$ is independent of x), together with point 1 above implies the flow will have no x-dependence, and indeed neither will the conformation tensor. Moreover, the change in pressure is taken to be only in the x-direction, so the only non-zero component of $\mathbf{u}$ is u_x. Therefore we have

$$\mathbf{u} = \mathbf{u}(t, r) = \begin{pmatrix} u_x(t, r) \\ 0 \\ 0 \end{pmatrix} \quad \text{and} \quad p = p(t, x); \;\; \partial_x p = f(t). \tag{4.1.1}$$

This will greatly simplify our work henceforth. Note that in cylindrical polars,

$$\nabla = \hat{\mathbf{i}}\nabla_x + \hat{\mathbf{r}}\nabla_r + \hat{\boldsymbol{\theta}}\nabla_\theta = \hat{\mathbf{i}}\partial_x + \hat{\mathbf{r}}\partial_r + \hat{\boldsymbol{\theta}}\frac{1}{r}\partial_\theta \tag{4.1.2}$$

and

$$\operatorname{div}(\mathbf{u}) = \partial_x u_x + \frac{1}{r}\partial_r(r u_r) + \frac{1}{r}\partial_\theta u_\theta \tag{4.1.3}$$

Notice that the configuration (4.1.1) naturally satisfies the continuity equation. For the momentum equation, we need to find the velocity gradient tensor $\boldsymbol{\nabla}\mathbf{u}$ and the divergence of the stress tensor $\nabla \cdot \boldsymbol{\sigma}$. We have that (adapted from [11])

$$\boldsymbol{\nabla}\mathbf{u} = \begin{pmatrix} \nabla u_{xx} & \nabla u_{xr} & \nabla u_{x\theta} \\ \nabla u_{rx} & \nabla u_{rr} & \nabla u_{r\theta} \\ \nabla u_{\theta x} & \nabla u_{\theta r} & \nabla u_{\theta\theta} \end{pmatrix} \tag{4.1.4}$$

where e.g.

$$\nabla u_{xr} := \nabla_x \mathbf{u} \cdot \hat{\mathbf{r}} = (\partial_x(u_x\hat{\mathbf{i}}) + \partial_x(u_r\hat{\mathbf{r}}) + \partial_x(u_\theta\hat{\boldsymbol{\theta}})) \cdot \hat{\mathbf{r}}.$$

Since

$$\begin{cases} \hat{\mathbf{r}} = \cos(\theta)\hat{\mathbf{j}} + \sin(\theta)\hat{\mathbf{k}} \\ \hat{\boldsymbol{\theta}} = -\sin(\theta)\hat{\mathbf{j}} + \cos(\theta)\hat{\mathbf{k}} \end{cases}$$

we see

$$\partial_\theta \hat{\mathbf{r}} = \hat{\boldsymbol{\theta}} \quad \text{and} \quad \partial_\theta \hat{\boldsymbol{\theta}} = -\hat{\mathbf{r}} \tag{4.1.5}$$

so that

$$\begin{cases} \nabla_x \mathbf{u} = \partial_x u_x \hat{\mathbf{i}} + \partial_x u_r \hat{\mathbf{r}} + \partial_x u_\theta \hat{\boldsymbol{\theta}} \\ \nabla_r \mathbf{u} = \partial_r u_x \hat{\mathbf{i}} + \partial_r u_r \hat{\mathbf{r}} + \partial_r u_\theta \hat{\boldsymbol{\theta}} \\ \nabla_\theta \mathbf{u} = \dfrac{1}{r}(\partial_\theta u_x \hat{\mathbf{i}} + \partial_\theta u_r \hat{\mathbf{r}} + u_r \hat{\boldsymbol{\theta}} + \partial_\theta u_\theta \hat{\boldsymbol{\theta}} - u_\theta \hat{\mathbf{r}}). \end{cases} \tag{4.1.6}$$

By using the product rule and substituting the result (4.1.4) and utilising that besides the relations in (4.1.4), other partials with respect to unit vectors are zero, it follows from orthonormality of the coordinate system that

$$\boldsymbol{\nabla}\mathbf{u} = \begin{pmatrix} \partial_x u_x & \partial_x u_r & \partial_x u_\theta \\ \partial_r u_x & \partial_r u_r & \partial_r u_\theta \\ \dfrac{1}{r}\partial_\theta u_x & \dfrac{1}{r}(\partial_\theta u_r - u_\theta) & \dfrac{1}{r}(\partial_\theta u_\theta + u_r) \end{pmatrix} \tag{4.1.7}$$

which, under (4.1.1), becomes

$$\boldsymbol{\nabla}\mathbf{u} = \begin{pmatrix} 0 & 0 & 0 \\ \partial_r u_x & 0 & 0 \\ 0 & 0 & 0 \end{pmatrix} \quad \text{and so} \quad \boldsymbol{\sigma} = \begin{pmatrix} -p & \mu\partial_r u_x & 0 \\ \mu\partial_r u_x & -p & 0 \\ 0 & 0 & -p \end{pmatrix}. \tag{4.1.8}$$

To find the divergence of the stress tensor in cylindrical coordinates, we need a more general definition [12]. Let us identify x, r and θ with 1, 2 and 3 and let $\widehat{\mathbf{e}}_i$ be the respective unit vectors so we can employ tensor notation. Similar to how we can derive (4.1.3) by writing

$$\operatorname{div}(\mathbf{u}) = \widehat{\mathbf{e}}_i \frac{1}{h_i} \cdot \partial_{x_i}(u_j \widehat{\mathbf{e}}_j) \tag{4.1.9}$$

and using the product rule, where $h_i = |\partial_{x_i}\mathbf{r}|$ are the length scales with $\mathbf{r} = x\hat{\mathbf{i}} + y\hat{\mathbf{j}} + z\hat{\mathbf{k}}$ an arbitrary position vector, we can too define, for a general form of $\boldsymbol{\sigma}$ (where $\otimes$ denotes the dyadic - equivalently

outer - product)

$$\nabla \cdot \boldsymbol{\sigma} = \widehat{\mathbf{e}}_i \frac{1}{h_i} \cdot \partial_{x_i} \left(\sigma_{jk} \widehat{\mathbf{e}}_j \otimes \widehat{\mathbf{e}}_k \right) \tag{4.1.10}$$

$$= \widehat{\mathbf{e}}_i \frac{1}{h_i} \cdot \left(\partial_{x_i} \left(\sigma_{jk} \right) \widehat{\mathbf{e}}_j \otimes \widehat{\mathbf{e}}_k + \sigma_{jk} \partial_{xi} \left(\widehat{\mathbf{e}}_j \right) \otimes \widehat{\mathbf{e}}_k + \sigma_{jk} \widehat{\mathbf{e}}_j \otimes \partial x_i \left(\widehat{\mathbf{e}}_k \right) \right)$$

$$= \frac{1}{h_i} \left(\partial_{x_i} \left(\sigma_{jk} \right) \left(\widehat{\mathbf{e}}_i \cdot \widehat{\mathbf{e}}_j \right) \widehat{\mathbf{e}}_k + \sigma_{jk} (\widehat{\mathbf{e}}_i \cdot \partial_{x_i} \left(\widehat{\mathbf{e}}_j \right)) \widehat{\mathbf{e}}_k + \sigma_{jk} \left(\widehat{\mathbf{e}}_i \cdot \widehat{\mathbf{e}}_j \right) \partial_{x_i} (\widehat{\mathbf{e}}_k) \right). \tag{4.1.11}$$

In the last line we used the observation that $u \cdot (v \otimes w) = (u \cdot v)w$. This is due to $[u \cdot (v \otimes w)]_j = u_i v_i w_j = [(u \cdot v)w]_j$ element-wise. Further, we recall that $\widehat{\mathbf{e}}_i \cdot \widehat{\mathbf{e}}_j = \delta_{ij}$, and $\partial_{x_i}(\widehat{\mathbf{e}}_j)$ is non-zero only when $i = 3$ i.e. partial with respect to θ and $j = 2, 3$. We deduce

$$\nabla \cdot \boldsymbol{\sigma} = \frac{1}{h_i} \partial_{x_i} \left(\sigma_{ik} \right) \widehat{\mathbf{e}}_k + \frac{1}{h_3} \sigma_{2k} \widehat{\mathbf{e}}_k + \frac{1}{h_3} \sigma_{3k} \partial_{x_3} \left(\widehat{\mathbf{e}}_k \right)$$

$$= \begin{pmatrix} \partial_x \sigma_{xx} + \frac{1}{r} \partial_r \left(r \sigma_{rx} \right) + \frac{1}{r} \partial_\theta \sigma_{\theta x} \\ \partial_x \sigma_{xr} + \frac{1}{r} \partial_r \left(r \sigma_{rr} \right) + \frac{1}{r} \partial_\theta \sigma_{\theta r} - \frac{1}{r} \sigma_{\theta\theta} \\ \partial_x \sigma_{x\theta} + \frac{1}{r} \partial_r \left(r \sigma_{r\theta} \right) + \frac{1}{r} \partial_\theta \sigma_{\theta\theta} + \frac{1}{r} \sigma_{\theta r} \end{pmatrix} \tag{4.1.12}$$

Therefore substituting the form of $\boldsymbol{\sigma}$ from (4.1.8), we arrive at

$$\nabla \cdot \boldsymbol{\sigma} = \begin{pmatrix} -\partial_x p \\ 0 \\ 0 \end{pmatrix} + \begin{pmatrix} \frac{\mu}{r} \partial_r (r \partial_r u_x) \\ 0 \\ 0 \end{pmatrix}. \tag{4.1.13}$$

On the LHS of the momentum equation we have an advection term $(\mathbf{u} \cdot \nabla)\mathbf{u}$; however, this equals zero by consideration of (4.1.1). Hence we are left with the momentum equation:

$$\rho \partial_t u_x = -\partial_x p + \mu \left(\partial_{rr} u_x + \frac{1}{r} \partial_r u_x \right) \tag{4.1.14}$$

To analyse the viscoelastic cases, we must also find the contribution of the polymer stress term as well as the corresponding equations for the Oldroyd-B model. In the case of cylindrical polar coordinates, the conformation tensor $\mathbf{A}$ becomes 3-by-3 symmetric. Using (4.1.12), we find the extra stress term is given by

$$\nabla \cdot (G\mathbf{A}) = G \begin{pmatrix} \frac{1}{r} \partial_r (r A_{xr}) \\ \frac{1}{r} \partial_r \left(r A_{rr} \right) - \frac{1}{r} A_{\theta\theta} \\ \frac{1}{r} \partial_r \left(r A_{r\theta} \right) + \frac{1}{r} A_{r\theta} \end{pmatrix}. \tag{4.1.15}$$

Recall that $\mathbf{A} = \mathbf{A}(t, r)$, so we see that $(\mathbf{u} \cdot \nabla)\mathbf{A} = 0$ on the LHS of (1.3.4). Substituting the form of $\boldsymbol{\nabla}\mathbf{u}$ from (4.1.8) into (1.3.4) yields a matrix equation from which we can read off the coveted PDEs for the 6 (due to symmetry) distinct entries of $\mathbf{A}$ - not all of which will be utilised by us, but

nonetheless presented here for completeness:

$$\begin{cases} \partial_t A_{xx} - 2A_{xr}\partial_r u_x = -\dfrac{1}{\tau}\left(A_{xx} - 1\right) \\ \partial_t A_{xr} - A_{rr}\partial_r u_x = -\dfrac{1}{\tau}A_{xr} \\ \partial_t A_{x\theta} - A_{r\theta}\partial_r u_x = -\dfrac{1}{\tau}A_{x\theta} \\ \partial_t A_{rr} = -\dfrac{1}{\tau}\left(A_{rr} - 1\right) \\ \partial_t A_{r\theta} = -\dfrac{1}{\tau}A_{r\theta} \\ \partial_t A_{\theta\theta} = -\dfrac{1}{\tau}\left(A_{\theta\theta} - 1\right) \end{cases} \tag{4.1.16}$$

4.2 Hagen-Poiseuille - Newtonian

We have mentioned that this case is the analog of the Poiseuille flow in a cylindrical pipe. There exists a constant pressure gradient $\partial_x p$ driving the flow, therefore we can make the additional simplification that $\mathbf{u} = \mathbf{u}(r)$ is independent of t. Hence (4.1.14) further simplifies to

$$\frac{\partial_x p}{\mu} = \partial_{rr} u_x + \frac{1}{r}\partial_r u_x \tag{4.2.1}$$

writing $v = \partial_r u_x$ and using the integrating factor r, we find

$$\begin{aligned} \frac{d}{dr}\left(rv\right) &= \frac{\partial_x p}{\mu} r \\ rv &= \frac{\partial_x p}{2\mu} r^2 + C_1 \end{aligned}$$

and we deduce from axisymmetry $v(0) = 0$ that $C_1 = 0$. Hence

$$u_x = \frac{\partial_x p}{4\mu} r^2 + C_2$$

Finally, we deploy the no-slip condition $u_x(R) = 0$ to arrive at

$$u_x(r) = \frac{\partial_x p}{4\mu}\left(r^2 - R^2\right) \tag{4.2.2}$$

Comparing this to the Poiseuille flow solution (2.3.4) with $R = H$ we observe they are nearly identical but for a factor of $1/2$. Intuitively this makes sense - the no-slip condition for Hagen-Poiseuille is all around the flow, whereas for Poiseuille it can be interpreted as only at the top and bottom, so we would expect the velocity to be slower given the same pressure gradient in the cylindrical pipe case.

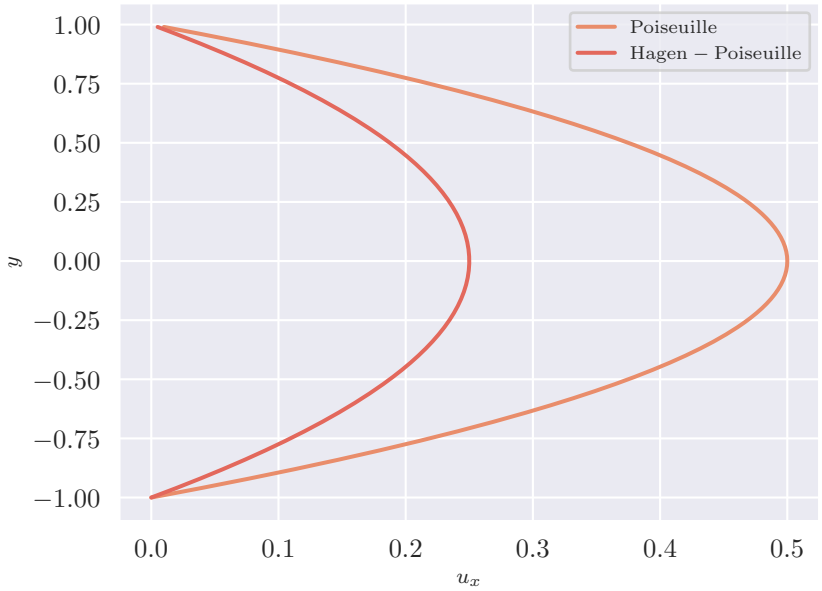

Figure 10: Velocity profile at $\partial_x p = -1$ and $\mu = 1$

4.3 Hagen-Poiseuille - Viscoelastic

Let us continue to examine the Hagen-Poiseuille flow - this time taking into account viscoelastic effects. (4.1.13) and (4.1.15) with (4.2.1) together give us the momentum equations

$$\begin{cases} \partial_x p = \mu \left(\partial_{rr} u_x + \frac{1}{r} \partial_r u_x \right) + \dfrac{G}{r} \partial_r (r A_{xr}) \\ 0 = \dfrac{G}{r} \partial_r \left(r A_{rr} \right) - \dfrac{G}{r} A_{\theta\theta} \\ 0 = \dfrac{G}{r} \partial_r \left(r A_{r\theta} \right) + \dfrac{G}{r} A_{r\theta} \end{cases} \tag{4.3.1}$$

As in the Newtonian problem, we have no time dependency for u_x, and hence by inspection of the first momentum equation, such is the case too for A_{xr}. The 2^{nd} conformation tensor equation provides further that A_{rr} is independent of t (this will force $A_{\theta\theta} = 1$, which fulfills the second momentum equation, and the third is not needed). We thus have

$$\begin{cases} A_{rr} \partial_r u_x = \dfrac{1}{\tau} A_{xr} \\ 0 = \dfrac{1}{\tau} (A_{rr} - 1) \end{cases} \tag{4.3.2}$$

which are readily solved to obtain

$$\begin{cases} A_{xr} = \tau \partial_r u_x \\ A_{rr} = 1 \end{cases} \tag{4.3.3}$$

Substituting into the first momentum equation yields

$$\begin{aligned}\partial_x p &= \mu\left(\partial_{rr}u_x + \frac{1}{r}\partial_r u_x\right) + \frac{G\tau}{r}\partial_r(r\partial_r u_x)\\ &= (\mu + G\tau)\left(\partial_{rr}u_x + \frac{1}{r}\partial_r u_x\right)\end{aligned} \tag{4.3.4}$$

This is exactly of the same form as the Newtonian case (4.2.1) and we have the same boundary conditions. Consequently we follow the same steps to arrive at

$$u_x(r) = \frac{\partial_x p}{4(\mu + G\tau)}\left(r^2 - R^2\right) \tag{4.3.5}$$

We notice the relationship between the Newtonian and viscoelastic case modelled by Oldroyd-B for Hagen-Poiseuille flow is identical to that for Poiseuille flow.

4.4 Periodic Pressure Gradient - Newtonian[2]

This subsection assumes blood to behave as a Newtonian fluid. To preserve generality, we do not further restrict the form of the pressure gradient $\partial_x p = f(t)$ as in (4.1.1) beyond the requirement of periodicity. Let the period of f be T and define an angular frequency

$$\omega_0 = \frac{2\pi}{T} \tag{4.4.1}$$

such that f can be expressed as a Fourier series with complex coefficients

$$f(t) = \sum_{n=-\infty}^{\infty} q_n e^{in\omega_0 t} \tag{4.4.2}$$

where $q_{-n} = \overline{q_n}$ as f is a real function. With this in mind, we may allow $\partial_x p = q_n e^{in\omega_0 t}$ for some arbitrary $n \neq 0$ (the $n = 0$ case is simply the Newtonian Hagen-Poiseuille solution). Our momentum equation is given by (4.1.14). Taking a Fourier time transform, on rearranging reveals

$$\partial_{rr}\hat{u}_x + \frac{1}{r}\partial_r\hat{u}_x - \frac{\rho\omega i}{\mu}\hat{u_x} = \frac{q_n}{\mu}\delta(\omega - n\omega_0) \tag{4.4.3}$$

The RHS is constant in r, so we find a particular integral

$$\hat{u}_x^{(P)} = \frac{q_n i}{\rho\omega}\delta(\omega - n\omega_0) \tag{4.4.4}$$

The homogeneous solution satisfies

$$r^2\partial_{rr}\hat{u}_x^{(H)} + r\partial_r\hat{u}_x^{(H)} - \frac{\rho\omega i}{\mu}r^2\hat{u}_x^{(H)} = 0 \tag{4.4.5}$$

which reduces to Bessel's differential equation

$$\zeta^2\partial_{\zeta\zeta}\hat{u}_x^{(H)} + \zeta\partial_\zeta\hat{u}_x^{(H)} + \zeta^2\hat{u}_x^{(H)} = 0 \tag{4.4.6}$$

[2]This particular configuration was discussed in [3, Chapter 16], the solution for which has been adapted to use the Fourier transform method

upon applying the substitution

$$\zeta = i\sqrt{\frac{\rho\omega i}{\mu}}r = i\lambda(\omega)r \tag{4.4.7}$$

with $\lambda(\omega)$ as in (3.1.11). Since this form of Bessel's differential equation has integer order 0, the general solution is written

$$\hat{u}_x^{(H)} = C_1(\omega)J_0\left(i\lambda(\omega)r\right) + C_2(\omega)Y_0\left(i\lambda(\omega)r\right) \tag{4.4.8}$$

and $\hat{u}_x = \hat{u}_x^{(H)} + \hat{u}_x^{(P)}$ where

$$J_0(x) = \sum_{m=0}^{\infty} \frac{(-1)^m}{(m!)^2}\left(\frac{x}{2}\right)^{2m} \tag{4.4.9}$$

$$Y_0(x) = \frac{2}{\pi}\left(J_0(x)\left(\gamma_E + \ln\left(\frac{x}{2}\right)\right) + \sum_{m=1}^{\infty} \frac{(-1)^{m-1}H_m}{(m!)^2}\left(\frac{x}{2}\right)^{2m}\right) \tag{4.4.10}$$

are Bessel functions of the first and second kind, respectively, of order 0. We observe that Y_0 has a singularity at $r = 0$, which implies $C_2(\omega) = 0$ as otherwise $\hat{ux}$ and u_x will also have this singularity (we do not allow this since we expect the velocity to be bounded). Applying the transformed boundary condition $\hat{u}_x(\omega, R) = 0$, we get

$$C_1(\omega) = \frac{-q_n i\delta(\omega - n\omega_0)}{\rho\omega J_0(i\lambda(\omega)R)}. \tag{4.4.11}$$

Therefore

$$\hat{u}_x(\omega, r) = \delta(\omega - n\omega_0)\frac{q_n i}{\rho\omega}\left(1 - \frac{J_0\left(i\lambda\left(\omega\right)r\right)}{J_0\left(i\lambda\left(\omega\right)R\right)}\right) \tag{4.4.12}$$

Taking the inverse transform,

$$\begin{aligned} u_x(t, r) &= \frac{1}{2\pi}\int_{\mathbb{R}} \hat{u}_x(\omega, r)e^{i\omega t}d\omega \\ &= \frac{q_n i}{2\rho n\omega_0}\left(1 - \frac{J_0\left(i\lambda\left(n\omega_0\right)r\right)}{J_0\left(i\lambda\left(n\omega_0\right)R\right)}\right)e^{in\omega_0 t} \end{aligned} \tag{4.4.13}$$

Let us write $v_n(t, r) := u_x(t, r)$ above. Then for $\partial_x p$ of the form (4.4.2), we possess the solution

$$\begin{aligned} u_x(t, r) &= \frac{q_0}{4\mu}(r^2 - R^2) + \sum_{n\in\mathbb{Z}\setminus\{0\}} v_n(t, r) \\ &= \frac{q_0}{4\mu}(r^2 - R^2) + \mathrm{Re}\left\{\sum_{n\in\mathbb{N}} \frac{q_n i}{\rho n\omega_0}\left(1 - \frac{J_0\left(i\lambda\left(n\omega_0\right)r\right)}{J_0\left(i\lambda\left(n\omega_0\right)R\right)}\right)e^{in\omega_0 t}\right\} \end{aligned} \tag{4.4.14}$$

wherein the solution for $n = 0$ derived in section 4.2 is added separately.

4.5 Periodic Pressure Gradient - Viscoelastic

Finally, we tackle the case where blood is considered to be viscoelastic, and we retain the same configuration for the periodic pressure gradient as in the previous section. From (4.1.14-4.1.15) we

educe

$$\begin{cases} \rho\partial_t u_x = -\partial_x p + \mu\left(\partial_{rr}u_x + \frac{1}{r}\partial_r u_x\right) + \dfrac{G}{r}\partial_r(rA_{xr}) \\ 0 = \dfrac{G}{r}\partial_r\left(rA_{rr}\right) - \dfrac{G}{r}A_{\theta\theta} \\ 0 = \dfrac{G}{r}\partial_r\left(rA_{r\theta}\right) + \dfrac{G}{r}A_{r\theta} \end{cases} \tag{4.5.1}$$

which are similar to the Hagen-Poiseuille equations, with a crucial distinction that our variables are now time-*dependent*. Indeed, the conformation tensor equations we require are

$$\begin{cases} \partial_t A_{xr} - A_{rr}\partial_r u_x = -\dfrac{1}{\tau}A_{xr} \\ \partial_t A_{rr} = -\dfrac{1}{\tau}\left(A_{rr} - 1\right) \end{cases} \tag{4.5.2}$$

so there is some more work to be done. We start by inspecting the latter of (4.5.2). This is first order separable, and solving yields (similar to the Cartesian case in section 3)

$$A_{rr} = 1 + F(r)e^{-t/\tau} \tag{4.5.3}$$

where F is an arbitrary function. Now as elements of $\mathbf{A}$ are physical quantities, $F(r)$ must be bounded. We argue again that as $\lim_{t\to\infty} A_{rr} = 1$, we can neglect the initial decay behaviour and assume $A_{rr}|_{t=0} = 1$ and hence $A_{rr} = 1$. Since $A_{\theta\theta}$ satisfies the same equation (6^{th} of (4.1.16)), by the same argument and assumption, it also equals one. Note these values indeed comply with the second momentum equation. Plugging what we found into the former of (4.5.2), we obtain upon Fourier transform in t,

$$\begin{cases} \left(i\omega + \dfrac{1}{\tau}\right)\hat{A}_{xr} = \partial_r\hat{u}_x \\ \left(i\omega + \dfrac{1}{\tau}\right)\partial_r\hat{A}_{xr} = \partial_{rr}\hat{u}_x \end{cases} \tag{4.5.4}$$

These can now be fed back into the Fourier transform of the first momentum equation to admit (with $n \neq 0$)

$$\rho\omega i\hat{u}_x = -q_n\delta(\omega - n\omega_0) + \mu(\partial_{rr}\hat{u}_x + \frac{1}{r}\partial_r\hat{u}_x) + G\left(\frac{\partial_r\hat{u}_x}{r\left(i\omega + \frac{1}{\tau}\right)} + \frac{\partial_{rr}\hat{u}_x}{\left(i\omega + \frac{1}{\tau}\right)}\right) \tag{4.5.5}$$

$$= -q_n\delta(\omega - n\omega_0) + \left(\mu + \frac{G}{i\omega + \frac{1}{\tau}}\right)(\partial_{rr}\hat{u}_x + \frac{1}{r}\partial_r\hat{u}_x). \tag{4.5.6}$$

Recalling the notation introduced in (3.2.7), we can write

$$\partial_{rr}\hat{u}_x + \frac{1}{r}\partial_r\hat{u}_x - \Lambda(\omega)\hat{ui}_x = -\frac{q_n i}{\rho\omega}\Lambda(\omega)\delta(\omega - n\omega_0) \tag{4.5.7}$$

from which we observe that the particular integral in the Newtonian case (4.4.4) remains a particular integral here. Furthermore, we again have that the homogeneous solution can be modified to fulfill Bessel's differential equation. Upon performing the analogous substitution

$$\xi = i\Lambda(\omega)r \tag{4.5.8}$$

the equation reduces to the same form as (4.4.6). With the same boundary conditions, the remainder of the solution follows as in the Newtonian case above. Let us denote

$$\nu_n(t,r) = \frac{q_n i}{2\rho n\omega_0}\left(1 - \frac{J_0\left(i\Lambda\left(n\omega_0\right)r\right)}{J_0\left(i\Lambda\left(n\omega_0\right)R\right)}\right)e^{in\omega_0 t} \tag{4.5.9}$$

If we write $\eta = \mu + G\tau$, adding back the $n = 0$ solution from section 4.3, we finally find the full solution as

$$\begin{aligned} u_x(t,r) &= \frac{q_0}{4\eta}(r^2 - R^2) + \sum_{n\in\mathbb{Z}\setminus\{0\}} \nu_n(t,r) \\ &= \frac{q_0}{4\eta}(r^2 - R^2) + \mathrm{Re}\left\{\sum_{n\in\mathbb{N}} \frac{q_n i}{\rho n\omega_0}\left(1 - \frac{J_0\left(i\Lambda\left(n\omega_0\right)r\right)}{J_0\left(i\Lambda\left(n\omega_0\right)R\right)}\right)e^{in\omega_0 t}\right\} \end{aligned} \tag{4.5.10}$$

4.6 Analysis and Comparisons

For lack of reliable experimental data, we use an empirical function to illustrate the validity of the derived analytical solution: we define $\partial_x p(t) = -ke^{-cx/2}\sin(cx)$, with $k > 0$ and $c = 3\pi/T$ shown in the figure below:

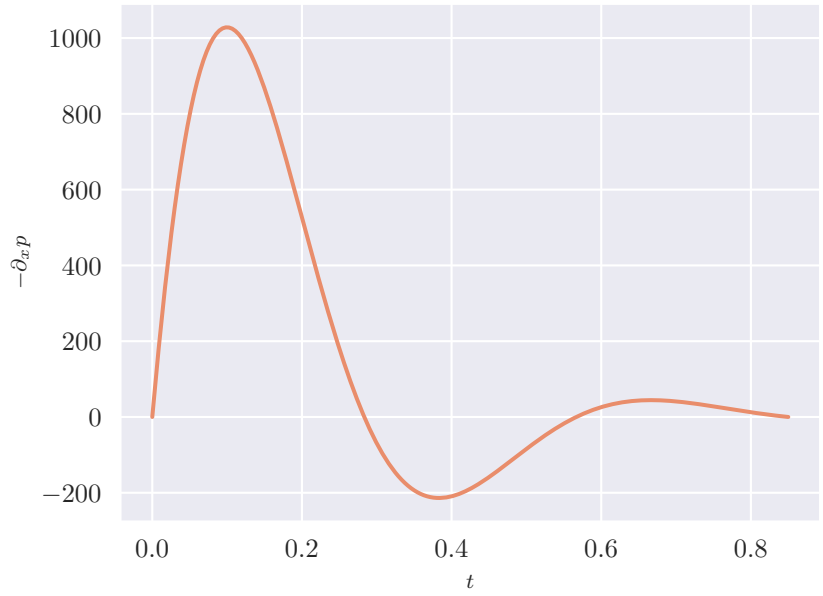

Figure 11: Negative pressure gradient (empirical) against time

We numerically compute its Fourier series coefficients q_n, and set the physical parameters somewhat arbitrarily:

Parameters	
T	0.85
R	0.025
ρ	1
ω_0	$\frac{2\pi}{T}$
μ	1

Presented are the 3D plots for one cycle (heartbeat) of the velocity. Left is the Newtonian case and right is the Oldroyd-B case. We chose slightly larger values $G = \tau = 10$ to highlight the effect of viscoelasticity on the flow. We see that in the viscoelastic case the velocities are clearly lower than in the Newtonian case (It should be noted that due to the 3D nature of the plots, it may appear that the velocity does not vanish at $r = R$, but in fact it does).

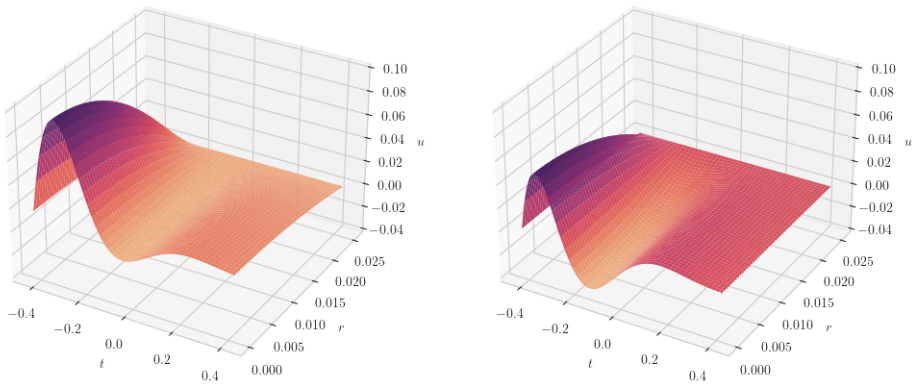

Figure 12: Velocity over one time period from $r = 0$ to $r = R$

Furthermore, the positive section of pressure gradient has a greater impact: the velocity becomes more negative in the viscoelastic case. We can interpret this as relating to the periodicity of $\partial_x p$ - the elasticity of the fluid exerts some stress towards the equilibrium position. We also present the cross sections of these plots in both r and t, which further clarify the situation.

We see that evidently in the Oldroyd-B case (right),

1. The velocities are lower overall

2. The velocity attains lower negative values

and we have omitted the legend for the r-cross-section plots due to its unwieldy size.

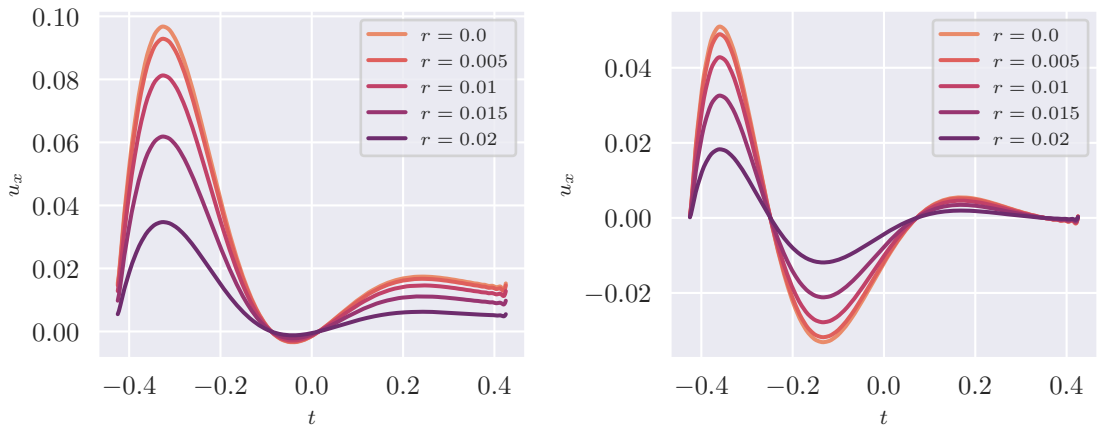

Figure 13: Velocity against t for varying values of r

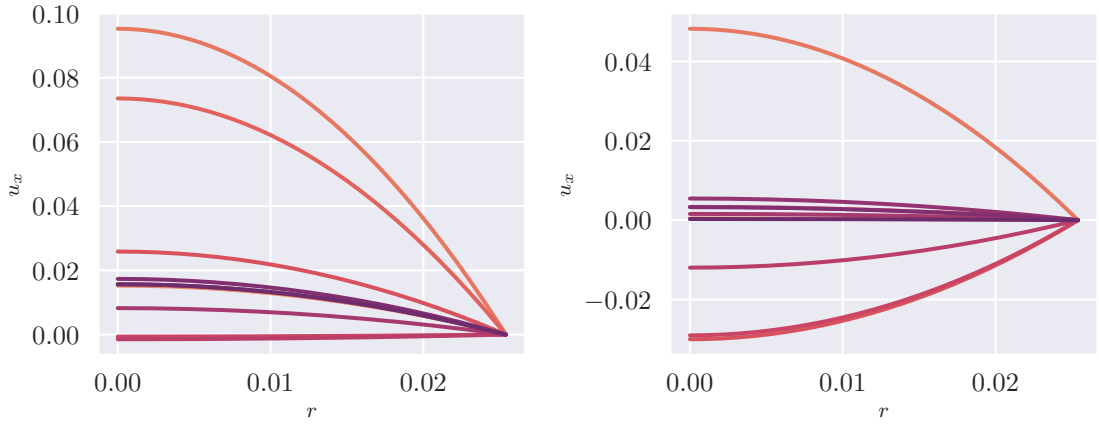

Figure 14: Velocity against r for varying values of t

4.7 Further Study

In our discussion of the blood flow problem, we have acknowledged that our assumptions limit our model so that it only reflects blood flow in certain long, straight arteries.

To further improve our model, we can consider a pressure gradient that more accurately reflects the pulse of a heart beat, perhaps by referencing experimentally obtained data. We could also consider the stretch and compression of the tissue forming the artery walls using Hooke's law. These two modelling assumptions allow us to expand our model to blood vessels such as the aorta, where the elasticity of walls are significant.

By using the Carreau model instead of the Oldroyd-B model, we could also capture the shear-thinning properties of blood. Additionally, the differing viscosities of the plasma and core flow can be considered to capture the fluid properties of blood more accurately.

5 Concluding Remarks and the Weissenberg Effect

The effect of the presence of polymers in a Newtonian fluid might not be significant in the previous cases, where we only highlighted the difference in the effective viscosity in a viscoelastic fluid and the viscosity in a Newtonian fluid, and often the velocity profiles can appear quite similar. However; in fact, there is another crucial difference between these types of fluids: the normal stress difference. We will illustrate it by looking at the rod climbing phenomenon, also known as the Weissenberg effect, which states that a viscoelastic fluid will be drawn up the rod instead of pushed away when a rod is rotated in the fluid. In the analysis of the rod climbing effect , the cylindrical coordinate system (z, r, θ) is used.

We consider a rod with radius a and a very long length rotating at a constant angular velocity Ω inside a very large pool of fluid (could be Newtonian or viscoelastic) on the surface of the Earth (with constant gravitational acceleration g). Since there is no time dependency in the boundary condition, we can assume that the flow is in a steady state. Throughout this section, we will impose the following conditions:

1. No-slip condition on the boundary of the rod:
$$\mathbf{u}_{r=a} = \begin{pmatrix} 0 \\ 0 \\ a\Omega \end{pmatrix}$$
2. Physically, we expect the fluid that is very far from the rod should not be affected by the rotating rod ($\mathbf{u}(\mathbf{r})_{r=\infty} = \mathbf{0}$).
3. From the boundary condition (1), we can deduce that there are no z or r dependencies in $\mathbf{u}$, so the only non-zero component should be the θ component. Additionally, since the problem is radially symmetric, we can assume that u_θ only depends on r. Combining the above, we have:
$$\mathbf{u} = \begin{pmatrix} 0 \\ 0 \\ u_\theta(r) \end{pmatrix}$$

Hence we have:
$$\nabla \mathbf{u} = \begin{pmatrix} 0 & 0 & 0 \\ 0 & 0 & \partial_r u_\theta \\ 0 & \frac{-u_\theta}{r} & 0 \end{pmatrix}$$

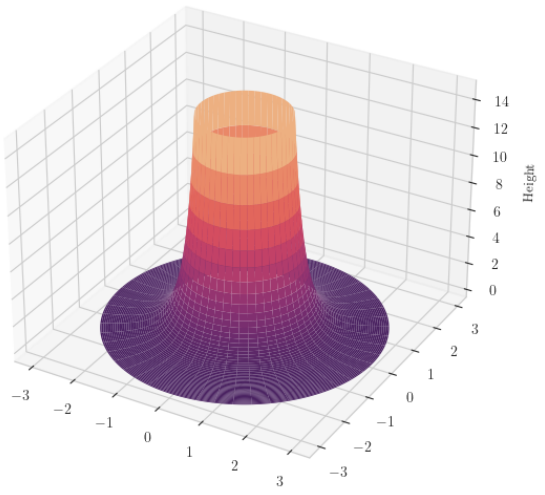

Figure 15: 3D plot of the Weissenberg 'rod climbing' effect for a viscoelastic fluid

As we know that the shear rate $\dot{\gamma} = \sqrt{2\mathbf{E} : \mathbf{E}}$ where $\mathbf{E} = \frac{1}{2}(\nabla \mathbf{u} + (\nabla \mathbf{u})^T)$
Thus

$$\dot{\gamma} = \partial_r u_\theta - \frac{u_\theta}{r}$$

5.1 Newtonian Case

Since the pressure of the fluid only depends on the depth of the fluid and how far it is from the rod, we have $p = p(z, r)$ and

$$\mathbf{u}(r) = \begin{pmatrix} 0 \\ 0 \\ u_\theta(r) \end{pmatrix}$$

And the three Navier-Stokes equations are

$$\begin{cases} 0 = -\partial_z p - \rho g \\ -\rho \dfrac{{u_\theta}^2}{r} = -\partial_r p \\ 0 = \mu \left(\dfrac{1}{r} \partial_r (r \partial_r u_\theta) - \dfrac{u_\theta}{r^2} \right) \end{cases} \tag{5.1.1}$$

Note that the third of these can be written as

$$0 = \mu \partial_r \left(\frac{1}{r} \partial_r (r u_\theta) \right)$$

Using the boundary conditions $u_\theta(a) = a\Omega$ and $u_\theta(\infty) = 0$ [13] yields

$$u_\theta = \frac{a^2\Omega}{r}$$

and

$$\dot{\gamma} = -\frac{2\Omega a^2}{r^2}$$

Using the second momentum equation,

$$p(z,r) = -\frac{\rho a^4 \Omega^2}{2r^2} + f(z) \tag{5.1.2}$$

And using first, we deduce

$$\partial_z \sigma_{zz} - \rho g = 0$$

Integrating with respect to z with boundary condition $p = 0$ at $z = h(r)$ [13], we get

$$p(z,r) = \rho g(h(r) - z)$$

We choose $f(z) = -\rho g z$ to eliminate the z dependence [13] in (5.1.2), we get

$$h(r) = -\frac{a^4\Omega^2}{2gr^2}$$

where $h(r)$ is the free surface height and $r \geq a$

5.2 Viscoelastic Case

To model a viscoelastic fluid, we will be using the Oldroyd-B. As before, we will start by solving for $\mathbf{A}$ using

$$\partial_t \mathbf{A} + (\mathbf{u}\cdot\nabla)\mathbf{A} - \mathbf{A}\cdot\nabla\mathbf{u} - (\nabla\mathbf{u})^T\cdot\mathbf{A} = -\frac{1}{\tau}(\mathbf{A} - \mathbf{I})$$

In this problem, time-dependence is absent, so $\mathbf{A} = \mathbf{A}(r)$ and $\mathbf{A}$ is symmetric

$$(\mathbf{u}\cdot\nabla)\mathbf{A} = \frac{u_\theta}{r}\begin{pmatrix} 0 & -A_{z\theta} & A_{zr} \\ -A_{z\theta} & -2A_{r\theta} & A_{rr} - A_{\theta\theta} \\ A_{zr} & A_{rr} - A_{\theta\theta} & 2A_{r\theta} \end{pmatrix}$$

$$\mathbf{A}\cdot\nabla\mathbf{u} = \begin{pmatrix} 0 & -A_{z\theta}\frac{u_\theta}{r} & A_{zr}\partial_r u_\theta \\ 0 & -A_{r\theta}\frac{u_\theta}{r} & A_{rr}\partial_r u_\theta \\ 0 & -A_{\theta\theta}\frac{u_\theta}{r} & A_{r\theta}\partial_r u_\theta \end{pmatrix}$$

$$(\nabla\mathbf{u})^T\cdot\mathbf{A} = \begin{pmatrix} 0 & 0 & 0 \\ -A_{z\theta}\frac{u_\theta}{r} & -A_{r\theta}\frac{u_\theta}{r} & -A_{\theta\theta}\frac{u_\theta}{r} \\ A_{zr}\partial_r u_\theta & A_{rr}\partial_r u_\theta & A_{r\theta}\partial_r u_\theta \end{pmatrix}$$

The equation then becomes

$$\begin{pmatrix} 0 & 0 & -A_{zr}\dot{\gamma} \\ 0 & 0 & -A_{rr}\dot{\gamma} \\ -A_{zr}\dot{\gamma} & -A_{rr}\dot{\gamma} & -2A_{r\theta}\dot{\gamma} \end{pmatrix} = -\frac{1}{\tau}\begin{pmatrix} A_{zz} - 1 & A_{zr} & A_{z\theta} \\ A_{zr} & A_{rr} - 1 & A_{r\theta} \\ A_{z\theta} & A_{r\theta} & A_{\theta\theta} - 1 \end{pmatrix}$$

Solving it component-wise, we get

$$\mathbf{A} = \begin{pmatrix} 1 & 0 & 0 \\ 0 & 1 & \tau\dot{\gamma} \\ 0 & \tau\dot{\gamma} & 1 + 2(\tau\dot{\gamma})^2 \end{pmatrix}$$

Coming back to the azimuthual component of the momentum equation

$$0 = \left(\nabla \cdot \begin{pmatrix} -p + G & 0 & 0 \\ 0 & -p + G & \eta\dot{\gamma} + GA_{r\theta} \\ 0 & \eta\dot{\gamma} + GA_{r\theta} & -p + GA_{\theta\theta} \end{pmatrix} \right)_\theta$$

$$(\eta + G\tau)\partial_{rr}u_\theta + \left(\frac{\eta + G\tau}{r}\right)\partial_r u_\theta - \left(\frac{\eta + G\tau}{r^2}\right)u_\theta = 0$$

Again, notice that it can be written as

$$0 = \partial_r \left(\frac{1}{r} \partial_r (r u_\theta) \right)$$

Using the same boundary conditions $u_\theta(a) = a\Omega$ and $u_\theta(\infty) = 0$ [13] yields

$$u_\theta = \frac{a^2\Omega}{r}$$

and

$$\dot{\gamma} = -\frac{2\Omega a^2}{r^2}$$

Now consider the radial component of the momentum equation

$$-\rho\frac{{u_\theta}^2}{r} = \partial_r \sigma_{rr} + \frac{\sigma_{rr} - \sigma_{\theta\theta}}{r} \tag{5.2.1}$$

Recall that $\sigma_{rr} = -p + G$ and $\sigma_{\theta\theta} = -p + G(1 + 2(\tau\dot{\gamma})^2)$, then (5.2.1) becomes

$$\partial_r p = \frac{\rho a^4 \Omega^2}{r^3} - \frac{8G\tau^2 a^4 \Omega^2}{r^5}$$

Integrating with respect to r yields

$$p(z, r) = -\frac{\rho a^4 \Omega^2}{2r^2} + \frac{2G\tau^2 a^4 \Omega^2}{r^4} + f(z) \tag{5.2.2}$$

Lastly, we consider the axial component but this time we do not ignore gravity

$$\partial_z \sigma_{zz} - \rho g = 0$$

Integrating with respect to z with boundary condition $p = 0$ at $z = h(r)$ [13]

$$p(z, r) = \rho g(h(r) - z)$$

We choose $f(z) = -\rho g z$ to eliminate the z dependence [13] in (5.2.2)

$$h(r) = \frac{1}{\rho g}\left(-a^4\Omega^2\left(\frac{\rho}{2r^2} - \frac{2G\tau^2}{r^4}\right)\right) \tag{5.2.3}$$

where $h(r)$ is the free surface height and $r \geq a$

5.3 Plots, Comparisons and Discussions

To account for this phenomenon physically, we observed that the height function $h(r)$ depends on the pressure function. At the surface of the fluid, i.e. $h(r)$, we have a balance between the atmospheric pressure and the fluid pressure. Therefore, if we have the pressure $p(r_A)$ be consistently greater than $p(r_B)$, see Figure 17.

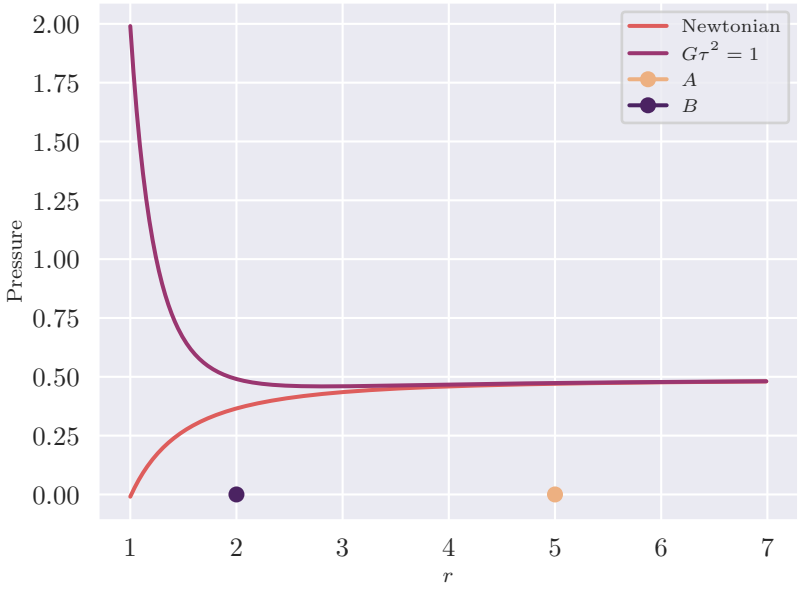

Figure 16: Pressure profile for a rotating rod at $z = -0.05$

For a fixed vertical position z we should expect the height of the fluid at r_A is higher than r_B since the extra pressure comes from the hydrostatic pressure generated by the fluid above it. To examine the relationship between the pressure and the vertical position z, we plotted the pressure-radius graph with various z. From Figure 19, it is clear that the pressure increases with z for all r where $p(z, r)$ is defined.

In the case of Newtonian fluids, the momentum equation in the radial direction (5.1.2) indicates that the pressure gradient in the r direction is always positive, which implies as the radial position r increases, the height would also increase.

However, in the case of a viscoelastic fluid, contrary to a Newtonian fluid, the normal stress difference in the r and θ is not zero and induces an outwards force, as seen in equation (5.2.1). We then expect the radial net force to increase as the elasticity of the viscoelastic fluid increases. Using (5.2.1) with given a and Ω, we can calculate the threshold of $G\tau^2$ for the effect to occur. In Figure 18, we can observe different degrees of the effect with varying $G\tau^2$. This causes the pressure gradient to be negative as $r \to a$, and this decreasing pressure together with $h(r) > 0$ as $r \to a$ are responsible for this phenomenon.[1]

One can also think about the pressure gradient by considering the net force of a control volume. We need the force generated by the normal stress difference to overcome the centripetal force for the

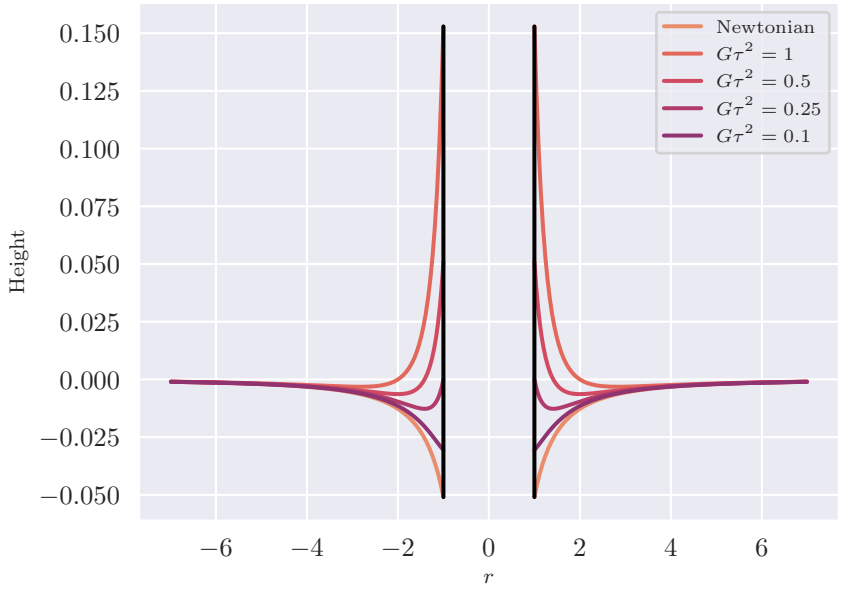

Figure 17: Height profile for a rotating rod for a Newtonian fluid and Oldroyd-B fluids with different parameters

effect to happen, which we can see from (5.2.1). Intuitively speaking, since the centripetal force is quadratically proportional to the velocity and inversely proportional to the radius, and recall that $u_\theta = \frac{a^2\Omega}{r}$, so we have the centripetal force is solely inversely proportional to r^3. The centripetal force is pointing towards the rod, which implies that the pressure increases with the radius, and the magnitude of the centripetal force is inversely proportional to r^3, which implies the gradient of the the pressure decreases with the radius. For a viscoelastic case using the Oldroyd-B model, we can see that from (5.2.1), $\frac{\sigma_{rr}-\sigma_{\theta\theta}}{r}$ is the force generated by the normal stress difference in the radial direction. If this force is greater than the centripetal force, we have a net force pointing radially outwards, which we can then use the same argument but with the direction reversed.

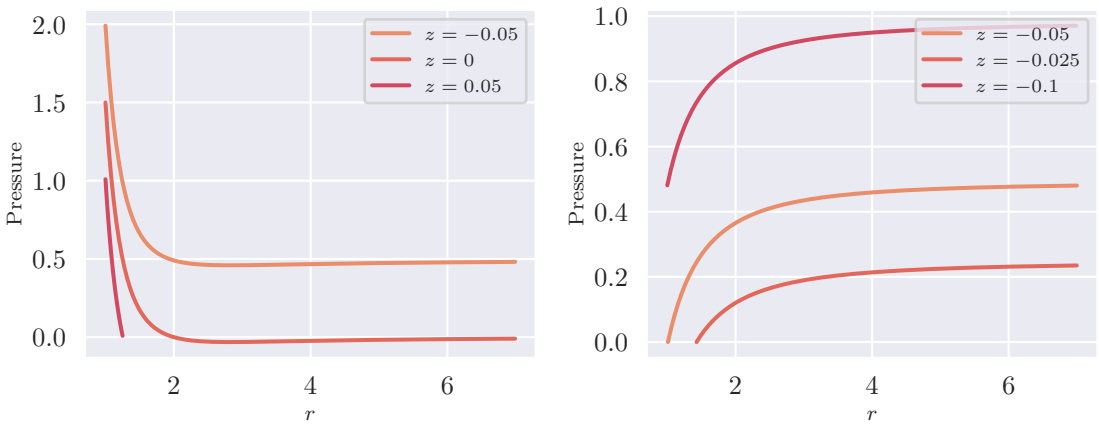

Figure 18: Pressure profile of an Oldroyd-B (left) fluid and Newtonian (right) fluid for a rotating rod

6 Appendix

Python code and links.

Note the second link contains a brief animation of the blood flow solution.
Link to the code for Carreau Model:
`https://github.com/MrJohnGalt-Pop/Carreau_numerical`
Link to the code for Graphs for Blood Flow, Rod Climbing and Poiseuille:
`https://github.com/MrJohnGalt-Pop/Fluid_graphs`

References

[1] Dr Helen J Wilson. Oldroyd-B fluid. Lecture, January 2006.

[2] Dr Helen J Wilson. Generalised Newtonian fluid. Lecture, January 2006.

[3] Pijush K. Kundu, Iram M. Cohen, and Favid R. Dowling. *Fluid Mechanics*. Elsevier Inc, London, 6th edition, 2016.

[4] Dr. Siddhartha Mishra and Dr. Franziska Weber. Topics in Mathematical and Computational Fluid Dynamics. Lecture, July 2016.

[5] Ain A Sonin. Equation of Motion for Viscous Fluids, 2001.

[6] Dr Helen J Wilson. Microscopic dynamics. Lecture, January 2006.

[7] PT Griffiths. Non-Newtonian channel flow — exact solutions. *IMA Journal of Applied Mathematics*, 85(2):263–279, 2020.

[8] Dr Helen J Wilson. Poiseuille Flow. Lecture, January 2006.

[9] H. P. Langtangen. A Primer on Scientific Programming with Python, 2016. Available from: `https://doi.org/10.1007/978-3-662-49887-3`.

[10] Malvern Panalytical. A Basic Introduction to Rheology, 2016.

[11] Jangsoe. Gradient tensor of vector in cylindrical coordinates, 2019. [Accessed 8 June 2023]. Available from: `https://blog.naver.com/richscskia/221744783715`.

[12] PA. Kelly. *Mechanics Lecture Notes: An introduction to Solid Mechanics*. Available from: `https://pkel015.connect.amazon.auckland.ac.nz/SolidMechanicsBooks/Part_III/Chapter_1_Vectors_Tensors/Vectors_Tensors_Complete.pdf`.

[13] John Hinch. Simple Flows. Lecture, October 2007. Available from: `https://www.damtp.cam.ac.uk/user/hinch/teaching/whoi/lecture03.ps`.

[14] F.Abraham, M.Behr, and M.Heinkenschloss. Shape optimisation in steady blood flow: A numerical study of non-Newtonian effects. *Computer Methods in Biomechanics and Biomedical Engineering*, 8(2):127–137, 2006. Available from: `https://doi.org/10.1080/10255840500180799`.

[15] Erwin Kreyszig. *Advanced Engineering Mathematics*. Laurie Rosatone, Jefferson City, 10th edition, 2011.

[16] Santhosh Kumar S and Somashekhar S. Hiremath. *The Role of Surface Modification on Bacterial Adhesion of Bio-implant Materials*, chapter 4. CRC Press, Boca Raton, 2020.